Singular limit analysis of a model for earthquake faulting

Bossolini, Elena; Brøns, Morten; Kristiansen, Kristian Uldall

Published in:
Nonlinearity

Publication date:
2017

Document Version
Early version, also known as pre-print

Singular limit analysis of a model for earthquake faulting

Elena Bossolini, Morten Brøns and Kristian Uldall Kristiansen

Department of Applied Mathematics and Computer Science, Technical University of Denmark, Kongens Lyngby 2800, DK

E-mail: ebos@dtu.dk, mobr@dtu.dk, krkri@dtu.dk

Abstract. In this paper we consider the one dimensional spring-block model describing earthquake faulting. By using geometric singular perturbation theory and the blow-up method we provide a detailed description of the periodicity of the earthquake episodes. In particular, the limit cycles arise from a degenerate Hopf bifurcation whose degeneracy is due to an underlying Hamiltonian structure that leads to large amplitude oscillations. We use a Poincaré compactification to study the system near infinity. At infinity the critical manifold loses hyperbolicity with an exponential rate. We use an adaptation of the blow-up method to recover the hyperbolicity. This enables the identification of a new attracting manifold that organises the dynamics at infinity. This in turn leads to the formulation of a conjecture on the behaviour of the limit cycles as the time-scale separation increases. We provide the basic foundation for the proof of this conjecture and illustrate our findings with numerics.

PACS numbers:

Keywords: singular perturbation; Hamiltonian systems; rate and state friction; blow-up; earthquake dynamics; Poincaré compactification

Submitted to: *Nonlinearity*

1. Introduction

Earthquake events are a non-linear multi-scale phenomenon. Some of the non-linearities that appear in earthquake faulting are fracture healing, repeating behaviour and memory effects (Ruina 1983, Heaton 1990, Vidale et al. 1994, Marone 1998*b*). In this paper we focus on the repeating behaviour of the earthquake cycles, where a cycle is defined as the combination of a rupture event with a following healing phase. An earthquake rupture consist of the instantaneous slipping of a fault side relative to the other side. The healing phase allows the fault to strengthen again and this process evolves on a longer time scale than the rupture event (Carlson & Langer 1989, Marone 1998*a*).

The repetition of the earthquake events is significant for the predictability of earthquake hazards. The data collected in the Parkfield experiment in California show evidence of recurring micro-earthquakes (Nadeau & McEvilly 1999, Marone et al. 1995, Bizzarri 2010, Zechar & Nadeau 2012). For large earthquakes it is harder to detect a repeating pattern from the data, even though recent works indicate the presence of recurring cycles (Ben-Zion 2008).

The one dimensional spring-block model together with the empirical Ruina friction law is a fundamental model to describe earthquake dynamics (Burridge & Knopoff 1967, Ruina 1983, Rice & Ruina 1983, Gu et al. 1984, Rice & Tse 1986, Carlson et al. 1991, Belardinelli & Belardinelli 1996, Ranjith & Rice 1999, Fan et al. 2014). Although the model does not represent all the non-linear phenomena of an earthquake rupture, it still reproduces the essential properties of the fault dynamics as extrapolated from experiments on rocks. The dimensionless form of the model is:

$$\begin{aligned} \dot{x} &= -\mathrm{e}^{z}\left(x + (1+\alpha)z\right), \\ \dot{y} &= \mathrm{e}^{z} - 1, \\ \varepsilon\dot{z} &= -\mathrm{e}^{-z}\left(y + \frac{x+z}{\xi}\right). \end{aligned} \tag{1}$$

System (1) has periodic solutions corresponding to the recurrence of the earthquake episodes, as shown in Figure 1 for two different values of the parameter ε and $\alpha > \xi$ fixed. The steep growth of the y-coordinate corresponds to the earthquake rupture, while the slow decay corresponds to the healing phase. Hence the periodic solutions of (1) have a multiple time-scale dynamics. Furthermore in Figure 1 we observe that the amplitude of the oscillations increases for decreasing

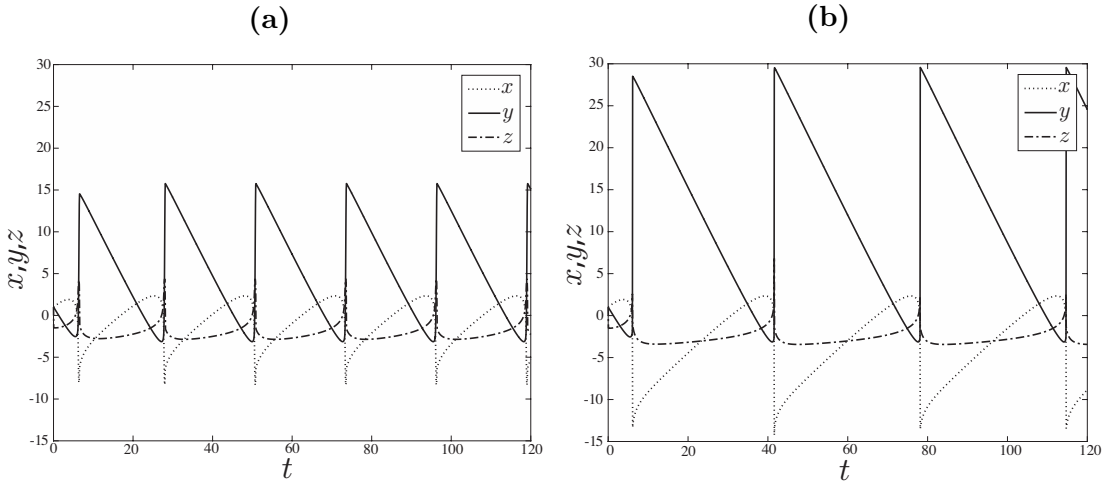

Figure 1: Numerical simulations of (1) for $\alpha = 0.9$ and $\xi = 0.5$. $\varepsilon = 10^{-2}$ in (a) while $\varepsilon = 10^{-5}$ in (b).

values of the time-scale separation ε. For these reasons extensive numerical simulations are difficult to perform in the relevant parameter range, that is $\varepsilon \ll 1$ (Rice & Tse 1986, Carlson & Langer 1989, Madariaga & Cochard 1996, Lapusta et al. 2000, Erickson et al. 2008, Erickson et al. 2011). We remark that the periodic solutions of (1) appear in a finite interval of values of $\alpha > \xi$. If α is much larger than ξ then chaotic dynamics emerges, as documented by Erickson et al. (2008).
It is the purpose of the present paper to initiate a rigorous mathematical study of (1) as a singular perturbation problem (Jones 1995, Kaper 1999). We will focus on the singular limit $\varepsilon = 0$. Our main result is the proof of the existence of an unbounded singular cycle when $\alpha > \xi$. For $\varepsilon > 0$ we provide enough arguments to expect this singular cycle to perturb into a stable, finite amplitude limit cycle, hence explaining the behaviour shown in Figure 1. In this way we can predict the periodic solutions of (1) even in parameter regions that are not possible to explore numerically. As we will see in section 3, our analysis is complicated by the fact that the critical manifold loses normal hyperbolicity at infinity with an exponential rate. This is a non-standard loss of hyperbolicity that also appears in other physical problems, like the ground dynamics of aircraft (Rankin et al. 2011). To deal with this issue we will first introduce a compactification of the phase space with the Poincaré sphere (Meiss 2007) and repeatedly use the blow-up method of Dumortier & Roussarie

(1996) in the version introduced by Krupa & Szmolyan (2001). For an extensive introduction to the blow-up method we refer to (Kuehn 2015).

Another way to study system (1) when $\varepsilon \ll 1$ is by using the method of matched asymptotic expansions, see (Eckhaus 1973) for an introduction. Putelat et al. (2008) have done the matching of the different time scales of (1) with an energy conservation argument, while in (Pomeau & Berre 2011) the causes of the switch between the two different time scales are not studied. However, the relaxation oscillation behavior of the periodic solutions of (1) is not explained.

Our paper is structured as follows. In section 2 we briefly discuss the physics of system (1). In section 3 we set (1) in the formalism of geometric singular perturbation theory and in section 4 we consider the analysis of the reduced problem for $\alpha = \xi$ and $\varepsilon = 0$. Here a degenerate Hopf bifurcation appears whose degeneracy is due to an underlying Hamiltonian structure that we identify. We derive the bifurcation diagram in section 5 after having introduced a compactification of the reduced problem. From this and from the analysis of section 6, we conclude that the limit cycles of Figure 1 cannot be described by the sole analysis of the reduced problem. In section 7 we present our main result on the existence of a singular unbounded cycle Γ_0. This leads to a conjecture, Conjecture 7.1, on the existence of limit cycles $\Gamma_\varepsilon \to \Gamma_0$ for $\varepsilon \ll 1$. The conjecture is supported by numerical simulations but in section 8 we also lay out the foundation of a proof by using the blow-up method to gain hyperbolicity of Γ_0. Finally in section 9 we conclude and summarize the results of our analysis.

2. Model

The one dimensional spring-block model is presented in Figure 2. We suppose that one fault side slides at a constant velocity v_0 and drags the other fault side of mass M through a spring of stiffness κ. The friction force $F_\mu = \sigma\mu$ acts against the motion. A common assumption is to suppose that the normal stress σ, i.e. the stress normal to the friction interface (Nakatani 2001), is constant $\sigma = 1$. The friction coefficient μ is modelled with the Ruina rate and state friction law $\mu = \mu(v, \theta)$, with v the sliding velocity and θ the *state* variable. The state θ accounts for how long the two surfaces have been in contact (Ruina 1983, Marone 1998*b*).

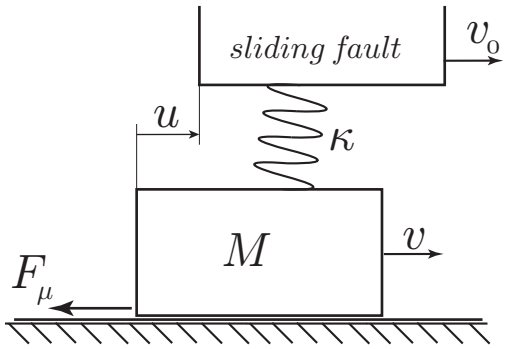

Figure 2: Spring-block model describing the earthquake faulting.

This gives rise to the following equations:

$$\begin{aligned} \theta' &= -\frac{v}{L}\left(\theta + b\ln\left(\frac{v}{v_0}\right)\right), \\ u' &= v - v_0, \\ v' &= -\frac{1}{M}\left(\kappa u + \left(\theta + a\ln\left(\frac{v}{v_0}\right)\right)\right), \end{aligned} \tag{2}$$

where the variable u is the relative displacement between the two fault sides and the prime denotes the time derivative. The parameter L is the characteristic displacement that is needed to recover the contact between the two surfaces when the slip occurs, while a and b are empirical coefficients that depend on the material properties (Marone 1998*b*).
System (2) is non-dimensionalized by introducing the new set of dimensionless coordinates (x, y, w, t) such that $\theta = ax,\ u = Ly,\ v = v_0 w,\ t = (v_0/L)t'$:

$$\begin{aligned} \dot{x} &= -w\left(x + (1+\alpha)\ln(w)\right), \\ \dot{y} &= w - 1, \\ \varepsilon\dot{w} &= -y - \frac{x + \ln(w)}{\xi}. \end{aligned} \tag{3}$$

We notice that equation (3) has a singularity in $w = 0$ and to avoid it we henceforth introduce the variable $z = \ln(w)$ so that we obtain the formulation presented in (1). In system (3) we have introduced the parameters: $\varepsilon = Mv_0^2/(\kappa L^2)$ such that $1/\sqrt{\varepsilon}$ is a non-dimensional frequency, $\xi = (\kappa L)/a$: the non-dimensional spring constant

and $\alpha = (b-a)/b$ describing the sensitivity to the velocity relaxation (Erickson et al. 2008). We consider the parameter values presented by Madariaga (1998): $\varepsilon \in [10^{-24}, 10^{-8}]$, $\xi = 0.5$, $\alpha > \xi$. A more extensive reference to the parameter sets can be found in the work of Dieterich (1972, 1978, 1979). In this paper we keep the parameter $\xi > 0$ fixed (we will use $\xi = 0.5$ in our computations) and we consider α as the bifurcation parameter. With this choice the study of (1) as a singular perturbation problem is simplified. Indeed as we will see in the following section 3, the critical manifold of (1) is a surface dependent on the parameter ξ. The results of our analysis can be easily interpreted for the case of α fixed and ξ varying, that is the standard approach in the literature.

3. Singular perturbation approach to the model

The positive constant $\varepsilon \ll 1$ in system (1) measures the separation of two time scales. In particular the variables (x, y) are slow while z is fast. We call equation (1) the slow problem and the dot refers to the differentiation with respect to the slow time t. We introduce the fast time $\tau = t/\varepsilon$ to obtain the fast problem:

$$\begin{aligned} x' &= -\varepsilon \mathrm{e}^z (x + (1+\alpha) z), \\ y' &= \varepsilon \left(\mathrm{e}^z - 1\right), \\ z' &= -\mathrm{e}^{-z} \left(y + \frac{x+z}{\xi}\right), \end{aligned} \tag{4}$$

where the prime stands for differentiation with respect to τ. The two systems (1) and (4) are equivalent whenever $\varepsilon > 0$. In the singular analysis we consider two different limit systems. By setting $\varepsilon = 0$ in (1) we obtain the reduced problem:

$$\begin{aligned} \dot{x} &= -\mathrm{e}^z (x + (1+\alpha) z), \\ \dot{y} &= \mathrm{e}^z - 1, \\ 0 &= -\mathrm{e}^{-z} \left(y + \frac{x+z}{\xi}\right), \end{aligned} \tag{5}$$

that is also referred in the literature as the quasi-static slip motion. Setting $\varepsilon = 0$ in (4) gives the layer problem:

$$z' = -\mathrm{e}^{-z} \left(y + \frac{x+z}{\xi}\right), \quad (x, y)(\tau) = (x^0, y^0). \tag{6}$$

System (6) has a plane of fixed points that we denote the critical manifold:

$$C_0 := \left\{(x, y, z) \in \mathbb{R}^3 \middle| \quad z = -x - \xi y\right\}, \tag{7}$$

this manifold is attracting, since:

$$\left.\frac{\partial z'}{\partial z}\right|_{C_0} = -\xi^{-1}\mathrm{e}^{-z} < 0. \tag{8}$$

The results by Fenichel (1974, 1979) guarantee that close to C_0 there is an attracting (due to (8)) slow-manifold S_ε for any compact set $(x, y) \in \mathbb{R}^2$ and ε sufficiently small. However we notice in (8) that C_0 loses its normal hyperbolicity at an exponential rate when $z \to +\infty$. This is a key complication: orbits leave a neighborhood of the critical manifold even if it is formally attracting. This is a non-standard loss of hyperbolicity that appears also in other physical problems such as the ground dynamics of aircraft (Rankin et al. 2011). To our knowledge, (Kristiansen 2016) is the first attempt on a theory of exponential loss of hyperbolicity. In the case of loss of hyperbolicity at an algebraic rate, like in the autocatalator problem studied originally by Gucwa & Szmolyan (2009), we refer to the work of Kuehn (2014).
Naïvely we notice that when $z \gg 1$ the dynamics of system (1) is driven by a new time scale, that is not related to its slow-fast structure. Assuming $z \gg \ln \varepsilon^{-1}$ we can rewrite (1) as:

$$\begin{aligned} \dot{x} &= -x - (1 + \alpha)z, \\ \dot{y} &= 1, \\ \dot{z} &= 0, \end{aligned} \tag{9}$$

where we have further rescaled the time by dividing the right hand side by e^z and ignored the higher order terms. Hence in this regime there is a family of x-nullclines:

$$x + (1 + \alpha)z = 0, \tag{10}$$

that are attracting since:

$$\frac{\partial \dot{x}}{\partial x} = -1.$$

This naïve approach is similar to the one used by Rice & Tse (1986) to describe the different time scales that appear in system (1).

4. Reduced Problem

We rewrite the reduced problem (5) as a vector field $f_0(y, z; \alpha)$ by elimination of x in (5):

$$f_0(y, z; \alpha) := \begin{cases} \dot{y} &= \mathrm{e}^z - 1, \\ \dot{z} &= \xi + \mathrm{e}^z \left(\alpha z - \xi y - \xi\right). \end{cases} \tag{11}$$

The following Proposition describes the degenerate Hopf bifurcation at the origin of (11) for $\alpha = \xi$.

Proposition 4.1 *The vector field (11) has an unique fixed point in $(y, z) = (0, 0)$ that undergoes a degenerate Hopf bifurcation for $\alpha = \xi$. In particular $f_0(y, z; \xi)$ is Hamiltonian and it can be rewritten as:*

$$f_0(y, z; \xi) = g(y, z) J \nabla H(y, z), \tag{12}$$

with

$$g(y, z) = \frac{\mathrm{e}^{\xi y + z}}{\xi}, \tag{13a}$$

$$H(y, z) = -\mathrm{e}^{-\xi y}\left(\xi y - \xi z + \xi + 1 - \xi \mathrm{e}^{-z}\right) + 1, \tag{13b}$$

and where J is the standard symplectic structure matrix: $J = \begin{bmatrix} 0 & 1 \\ -1 & 0 \end{bmatrix}$.

Proof The linear stability analysis of (11) in the fixed point $(y, z) = (0, 0)$ gives the following Jacobian matrix:

$$D f_0(0, 0; \alpha) = \begin{bmatrix} 0 & 1 \\ -\xi & \alpha - \xi \end{bmatrix}. \tag{14}$$

The trace of (14) is zero for $\alpha = \xi$ and its determinant is $\xi > 0$. Hence a Hopf bifurcation occurs. The direct substitution of (13) into (12) shows that system (11) is Hamiltonian for $\alpha = \xi$. Therefore the Hopf bifurcation is degenerate. □

The Hopf bifurcation of (11) for $\alpha = \xi$ is a known result (Ruina 1983, Putelat et al. 2008, Erickson et al. 2008). The Hamiltonian function $H(y, z)$ has been used as a Lyapunov function in (Gu et al. 1984) without realising the Hamiltonian structure of the system. From Proposition 4.1 we obtain a vertical family of periodic orbits

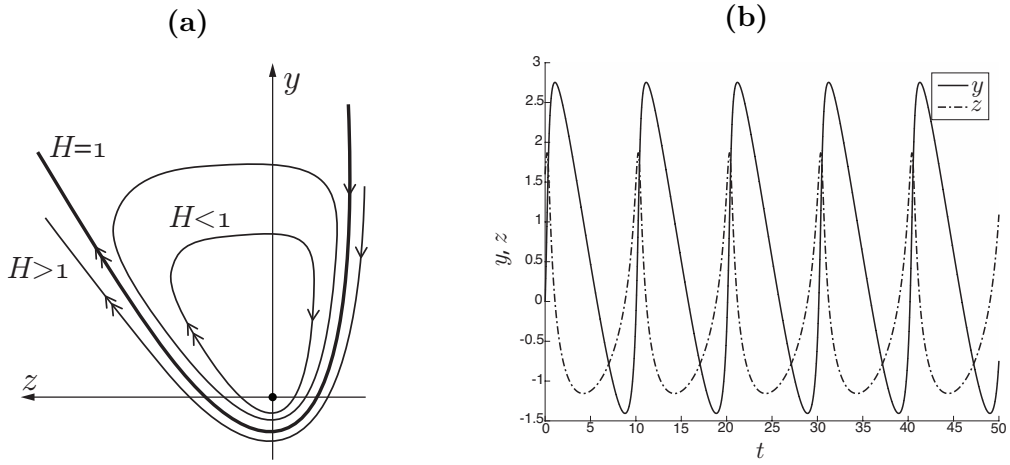

Figure 3: Behaviour of the reduced problem (12) for $\alpha = \xi$. In (a): phase space. The axis orientation is chosen in order to be consistent with the remaining figures of the paper. In (b): simulation of (12) for $H = 0.4,\ \xi = 0.5$.

for $\alpha = \xi$. The phase space of (12) is illustrated in figure 3(a) for positive values of $H(y, z)$. We remark that the fixed point $(y, z) = (0, 0)$ is associated with $H(y, z) = 0$. The intersection of the y-axis with the orbits $H(y, z) = h$ corresponds to the real roots of the Lambert equation:

$$-\,\mathrm{e}^{-\xi y}(\xi y + 1) + 1 = h, \quad h \geq 0. \tag{15}$$

Equation (15) has a real root for any $h > 0$ in the region $y < 0$, while a second real root in the region $y > 0$ exists only for $h \in (0, 1)$ (Corless et al. 1996). The intersection of the Hamiltonian trajectories with the y-axis is transversal for all $h > 0$, since the following condition holds:

$$\frac{\partial H}{\partial y}(y, 0) = \xi^2 y \mathrm{e}^{-\xi y} \neq 0, \quad \forall y \neq 0. \tag{16}$$

The trajectory identified with $H(y, z) = 1$ plays a special role because it separates the closed orbits for $H \in (0, 1)$ from the unbounded orbits for $H \geq 1$.

Remark 1 *From (16) it follows that the function $H(y, 0)$ defines a diffeomorphism between the points on the positive y-axis and the corresponding values $h \in (0, 1)$.*

Figure 3(b) highlights that the reduced problem (12) has an intrinsic slow-fastness. Indeed the phase space of (12) is swept with different speeds depending on the

region considered. This feature is represented in Figure 3(a), with the double arrow representing fast motion. In particular when $z > 0$ the trajectories are swept faster than for $z < 0$. This is due to the exponential function in (11). The fast sweep for $z > 0$ corresponds to the steep increase in the y coordinate of Figure 3(b). This fast dynamics for $z > 0$ resembles the slip that happens during an earthquake rupture, while the slow motion for $z < 0$ matches the healing phase, recall Figure 1. From this observation we tend to disagree with the notation used in the literature, that calls the reduced problem the quasi-static phase.
In order to describe the unbounded trajectories with $H(y, z) \geq 1$ for $y, z \to \infty$ and to extend the analysis to the case $\alpha \neq \xi$, we introduce a compactification of the reduced problem (11) and then we rewrite (11) on the Poincaré sphere.

5. Compactification of the reduced problem

We define the Poincaré sphere $\mathcal{S}^{2,+}$ as:

$$\mathcal{S}^{2,+} := \{(Y, Z, W) \in \mathbb{R}^3 \big| \quad Y^2 + Z^2 + W^2 = 1, \quad W \geq 0\}, \tag{17}$$

which projects the phase space of (11) onto the northern hemisphere of $\mathcal{S}^{2,+}$. Geometrically this corresponds to embedding (11) into the plane $W = 1$ that we call the directional chart k_2:

$$k_2 := \mathcal{S}^{2,+} \cap \{W = 1\}, \quad y_2 = \frac{Y}{W}, \; z_2 = \frac{Z}{W},$$

and the dynamics on chart k_2 follows directly from (11) by variable substitution:

$$\begin{aligned} \dot{y}_2 &= \mathrm{e}^{z_2} - 1, \\ \dot{z}_2 &= \xi + \mathrm{e}^{z_2} \left(\alpha z_2 - \xi y_2 - \xi\right). \end{aligned} \tag{18}$$

The points at infinity in k_2 correspond to the condition $W = 0$, that is the equator of $\mathcal{S}^{2,+}$. To study the dynamics on the equator we introduce the two additional directional charts:

$$k_3 := \mathcal{S}^{2,+} \cap \{Z = 1\}, \quad y_3 = \frac{Y}{Z}, w_3 = \frac{W}{Z}, \tag{19a}$$

$$k_1 := \mathcal{S}^{2,+} \cap \{Y = 1\}, \quad z_1 = \frac{Z}{Y}, w_1 = \frac{W}{Y}. \tag{19b}$$

We follow the standard convention of Krupa & Szmolyan (2001) and use the subscript $i = 1, 2, 3$ to denote a quantity in chart k_i. We denote with k_{ij} the transformation from chart k_i to chart k_j for $i, j = 1, 2, 3$. We have the following change of coordinates:

$$k_{23}: \quad w_3 = z_2^{-1}, \quad y_3 = y_2 z_2^{-1}, \tag{20a}$$

$$k_{21}: \quad w_1 = y_2^{-1}, \quad z_1 = z_2 y_2^{-1}, \tag{20b}$$

$$k_{31}: \quad w_1 = w_3 y_3^{-1}, \quad z_1 = y_3^{-1}, \tag{20c}$$

that are defined for $z_2 > 0$, $y_2 > 0$ and $y_3 > 0$ respectively. The inverse transformations $k_{ji} = k_{ij}^{-1}$ are defined similarly. Figure 4 shows a graphical representation of the sphere and of the directional charts.
We define $C_{0,\infty}$ as the extension of the critical manifold C_0 onto the equator of the sphere. From (8) it follows that $C_{0,\infty}$ is non-hyperbolic.

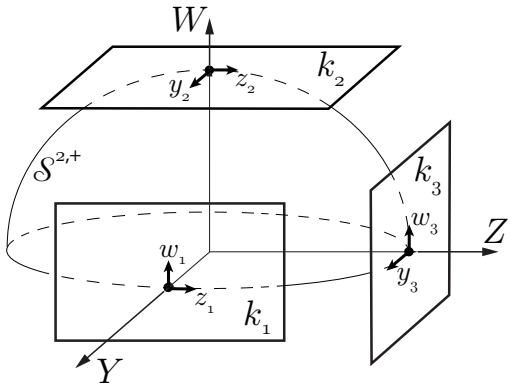

Figure 4: Poincaré sphere $\mathcal{S}^{2,+}$ and the directional charts $k_{1,2,3}$.

Proposition 5.1 *There exist transformations of time, that are smooth for $W > 0$ and that de-singularize the dynamics within $W = 0$, so that the reduced problem (11) has four fixed points $Q^{1,3,6,7}$ on $C_{0,\infty}$ satisfying:*

- *Q^1 is an improper stable node with a single eigenvector tangent to $C_{0,\infty}$.*
- *Q^3 has one unstable direction that is tangent to $C_{0,\infty}$ and a unique center-stable manifold $W^{c,s}$.*
- *Q^6 has one stable direction that is tangent to $C_{0,\infty}$ and a unique center-unstable manifold $W^{c,u}$.*

- Q^7 *is an improper unstable node with a single eigenvector tangent to* $C_{0,\infty}$.

The stability properties of the fixed points are independent of α*, in particular both* $W^{c,s}$ *and* $W^{c,u}$ *are smooth in* α.

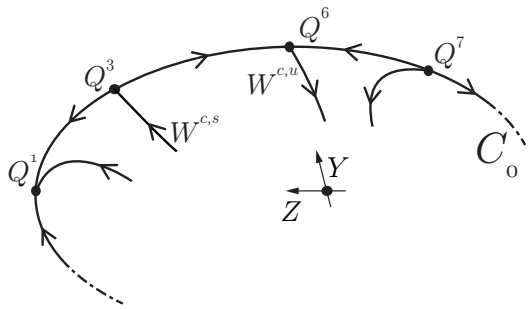

Figure 5: Fixed points on the compactified critical manifold C_0.

Figure 5 gives a representation of the statements of Proposition 5.1. We remark that we use superscripts as enumeration of the points $Q^m, m = 1, 3, 6, 7$ to avoid confusion with the subscripts that we have used to define the charts $k_i, i = 1, 2, 3$. In particular the enumeration choice of the superscripts will become clear in section 7, where we will introduce the remaining points $Q^{2,4,5}$ in (53). In Proposition 5.2 we relate the structure at infinity of (11) to the dynamics on C_0 with respect to the bifurcation parameter α.

Proposition 5.2 *Fix* $c > 0$ *small and consider the parameter interval:*

$$\alpha \in [\xi - c, \xi + c]. \tag{21}$$

Then Figure 6 describes the phase space of (11) *with respect to* α*. In particular:*

- *When* $\alpha < \xi$ *the set* $W^{c,s}$ *separates the basin of attraction of* $(y, z) = (0, 0)$ *from the solutions that are forward asymptotic to* Q^1.
- *When* $\alpha = \xi$ *Proposition 4.1 holds. The set* $H = 1$ *corresponds to* $W^{c,s} \cap W^{c,u}$.
- *When* $\alpha > \xi$ *the set* $W^{c,u}$ *separates the solutions that are backwards asymptotic to the origin to the ones that are backwards asymptotic to* Q^7.

Therefore no limit cycles appear in the reduced problem for $\varepsilon = 0$ *and* $\alpha \neq \xi$.

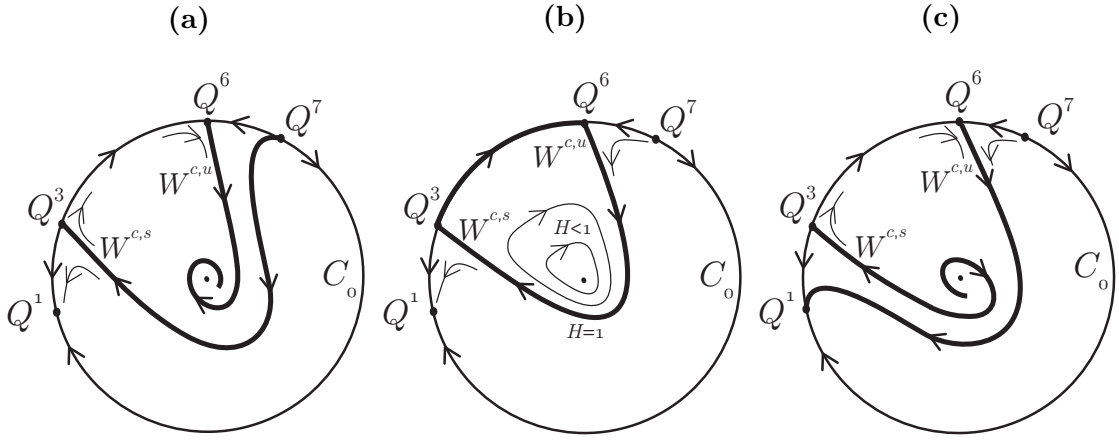

Figure 6: Bifurcation diagram of (11) with respect to the parameter α. Orbits spiral inwards for $\alpha < \xi$ (a) or outwards for $\alpha > \xi$ (c). In (b): $\alpha = \xi$.

Remark 2 *The local stability analysis of* $(y, z) = (0, 0)$ *can be directly obtained using* $H(y, z)$ *as a Lyapunov function. This was done in (Gu et al. 1984).*

In the rest of the section we prove the previous two propositions. In sections 5.1 and 5.2 we perform an analysis of (11) in the two charts k_3 and k_1 respectively to show Proposition 5.1. We prove Proposition 5.2 in section 5.3.

5.1. Chart k_3

We insert (19a) into the reduced problem (18) and obtain the following system:

$$\begin{aligned} \dot{w}_3 &= -w_3(\alpha - \xi y_3) + \xi w_3^2(1 - \mathrm{e}^{-\frac{1}{w_3}}), \\ \dot{y}_3 &= -y_3(\alpha - \xi y_3) - w_3(1 + \xi y_3)(1 - \mathrm{e}^{-\frac{1}{w_3}}), \end{aligned} \tag{22}$$

here we have divided the right hand side by $\exp(1/w_3)$ to de-singularize $w_3 = 0$.

Remark 3 *The division by* $\exp(1/w_3)$ *in* (22) *is formally performed by introducing the new time* t_3 *such that:*

$$\mathrm{d}t_3 = \exp(1/w_3)\mathrm{d}t. \tag{23}$$

A similar de-singularization procedure is used also in the blow-up method.

System (22) has two fixed points:

$$Q^1 := \quad (w_3, y_3) = (0, 0), \tag{24a}$$

$$Q^3 := \quad (w_3, y_3) = \left(0, \frac{\alpha}{\xi}\right). \tag{24b}$$

The point Q^1 is a stable improper node with the double eigenvalue $-\alpha$ and a single eigenvector $(0,1)^T$. The point Q^3 has one unstable direction $(0,1)^T$ due to the positive eigenvalue α and a center direction $(\alpha/(1+\alpha), 1)^T$ due to a zero eigenvalue. Notice that for $\alpha = \xi$ then $Q^3 = (0,1)$.

Lemma 5.3 *There exists a unique center-stable manifold $W^{c,s}$ at the point Q^3. This manifold is smooth in α. For $\alpha = \xi$ the set $H = 1$ coincides with $W^{c,s}$.*

Proof For $\alpha = \xi$ we rewrite the Hamiltonian (13b) in chart k_3 and insert the condition $H = 1$ to obtain the implicit equation:

$$\xi(y_3 - 1) + w_3(\xi + 1) - \xi w_3 \mathrm{e}^{-\frac{1}{w_3}} = 0, \tag{25}$$

then $w_3 \to 0$ gives $y_3 \to 1$ that is the point Q^3. As a consequence Q^3 has a saddle-like behaviour with an unique center-stable manifold $W^{c,s}$ tangent to $(\alpha/(1+\alpha), 1)^T$. This invariant manifold $W^{c,s}$ is smooth in α and therefore it preserves its features for small variations of α from $\alpha = \xi$. □

Remark 4 *With respect to t_3 the points within $W^{c,s}$ decay algebraically to Q^3, while the decay towards the stable node Q^1 is exponential. Using (23) it then follows that all these points reach $w_3 = 0$ in finite time with respect to the original slow time t. This is a formal proof of the finite time blow-up of solutions of (11) for $\alpha > \xi$ that was also observed by Gu et al. (1984) and by Pomeau & Berre (2011).*

5.2. Chart k_1

We insert (19b) into the reduced problem (18) to obtain the dynamics in chart k_1:

$$\begin{aligned} \dot{w} &= w^2(1 - \mathrm{e}^{\frac{z}{w}}), \\ \dot{z} &= w(\xi + z)(1 - \mathrm{e}^{\frac{z}{w}}) + \mathrm{e}^{\frac{z}{w}}(\alpha z - \xi), \end{aligned} \tag{26}$$

where we have dropped the subscript for the sake of readability. We observe that the exponential term in (26) is not well defined in the origin. For this reason we introduce the blow-up transformation:

$$w = \bar{r}\bar{\omega}, \qquad z = \bar{r}\bar{\zeta}, \tag{27}$$

where $(\bar{\omega}, \bar{\zeta}) \in S^1 = \{(\bar{\omega}, \bar{\zeta}) : \bar{\omega}^2 + \bar{\zeta}^2 = 1\}$ and $\bar{r} \geq 0$. We consider the following charts:

$$\kappa_1 : \quad w = r_1\omega_1, \quad z = r_1, \tag{28a}$$
$$\kappa_2 : \quad w = r_2, \quad z = r_2\zeta_2, \tag{28b}$$
$$\kappa_3 : \quad w = r_3\omega_3, \quad z = -r_3. \tag{28c}$$

Next we perform an analysis of the blown-up vector field and the main results are summarized in Figure 7.

Chart κ_1 We insert condition (28a) into system (26) and divide the right hand side by $\exp(1/\omega_1)/r_1$ to get the de-singularized dynamics in chart κ_1:

$$\begin{aligned} \dot{\omega}_1 &= \omega_1(\xi - \alpha r_1) + r_1\omega_1^2\xi\left(1 - \mathrm{e}^{-\frac{1}{\omega_1}}\right), \\ \dot{r}_1 &= -r_1(\xi - \alpha r_1) - r_1^2\omega_1(\xi + r_1)\left(1 - \mathrm{e}^{-\frac{1}{\omega_1}}\right). \end{aligned} \tag{29}$$

System (29) has one fixed point in $(\omega_1, r_1) = (0, \xi/\alpha)$ that corresponds to the point Q^3 introduced in (24b). Furthermore system (29) has a second fixed point in $O_1 := (\omega_1, r_1) = (0, 0)$ with eigenvalues ξ, $-\xi$ and corresponding eigenvectors $(1, 0)^T$ and $(0, 1)^T$. Both the eigendirections of O_1 are invariant and we denote by γ_1 the heteroclinic connection between Q^3 and O_1 along the r_1-axis.
The initial condition $p_{1,\text{in}}$ on $W^{c,s}$ with $\omega_1 = \delta > 0$ is connected through the stable and the unstable manifolds of O_1 to the point $p_{1,\text{out}} := (\omega_1, r_1) = (\delta^{-1}, 0)$ as shown in Figure 7(a).

Chart κ_2 We insert the transformation (28b) into (26) and divide the right hand side by $\exp(\zeta_2)/r_2$ to obtain the de-singularized vector field in chart κ_2. In this chart there are no fixed points, however the line $r_2 = 0$ is invariant and ζ_2 is monotonically decreasing along it. The orbit entering from chart κ_1 has the initial

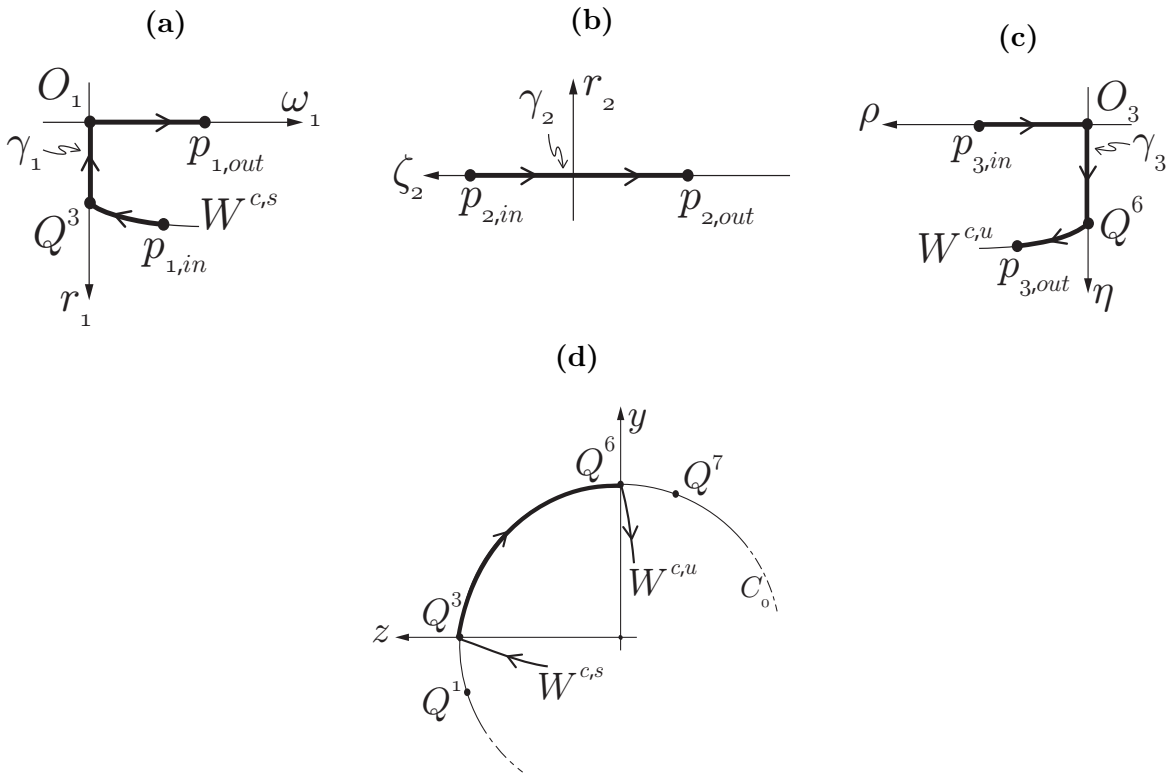

Figure 7: Blow-up of (26) in chart k_1. (a), (b) and (c) represent charts κ_1, κ_2 and κ_3 respectively. In (d): behaviour at infinity after the blow-down.

condition $p_{2,\text{in}} := \kappa_{12}(p_{1,\text{out}}) = (\zeta_2, r_2) = (\delta, 0)$ that lies on the invariant line $r_2 = 0$. Thus the solution starting in $p_{2,\text{in}}$ evolves up to the point $p_{2,\text{out}} := (\zeta_2, r_2) = (-\delta^{-1}, 0)$, as shown in Figure 7(b).

Chart κ_3 We introduce condition (28c) into the vector field (26) and divide by w_3 to obtain the de-singularized dynamics in chart κ_3:

$$\begin{aligned} \dot{\omega}_3 &= (\xi - r_3)(1 - \mathrm{e}^{-\frac{1}{\omega_3}}) + r_3\omega_3(1 - \mathrm{e}^{-\frac{1}{\omega_3}}) + \frac{\mathrm{e}^{-\frac{1}{\omega_3}}}{r_3}(\alpha r_3 + \xi), \\ \dot{r}_3 &= -r_3(\xi - r_3)(1 - \mathrm{e}^{-\frac{1}{\omega_3}}) - \frac{\mathrm{e}^{-\frac{1}{\omega_3}}}{\omega_3}(\alpha r_3 + \xi). \end{aligned} \tag{30}$$

System (30) has an unstable improper node in:

$$Q^7 := \quad (\omega_3, r_3) = (0, \xi), \tag{31}$$

with double eigenvalue ξ and single eigenvector $(1,0)^T$. For $w_3 = r_3 = 0$ the quantity $\mathrm{e}^{-1/\omega_3}/r_3$ in (30) is not well defined. We deal with this singularity by first multiplying the right hand side of the vector field by $r_3\omega_3$:

$$\begin{aligned}\dot{\omega}_3 &= r_3\omega_3(\xi - r_3)(1 - \mathrm{e}^{-\frac{1}{\omega_3}}) + r_3^2\omega_3^2(1 - \mathrm{e}^{-\frac{1}{\omega_3}}) + \omega_3\mathrm{e}^{-\frac{1}{\omega_3}}(\alpha r_3 + \xi),\\ \dot{r}_3 &= -r_3^2\omega_3(\xi - r_3)(1 - \mathrm{e}^{-\frac{1}{\omega_3}}) - r_3\mathrm{e}^{-\frac{1}{\omega_3}}(\alpha r_3 + \xi).\end{aligned} \tag{32}$$

Next we introduce the blow-up transformation:

$$\omega_3 = \rho, \qquad r_3 = \frac{\mathrm{e}^{-1/\rho}}{\rho}\eta. \tag{33}$$

We substitute (33) into (32) and we divide by $\exp(-1/\rho)/\rho$ to obtain the desingularized vector field:

$$\begin{aligned}\dot{\rho} &= \xi\rho^2(\eta - 1) + \mathrm{O}\left(\frac{\eta}{\rho}\mathrm{e}^{-1/\rho}\right),\\ \dot{\eta} &= -\eta\xi(\eta - 1) + \mathrm{O}\left(\frac{\eta}{\rho}\mathrm{e}^{-1/\rho}\right).\end{aligned} \tag{34}$$

Remark 5 *The blow-up map (33) is non-standard, since it is not written as an algebraic expression in ρ. We will encounter a similar difficulty in section 7, where in order to blow-up the vector field we will increase the phase space dimension by one.*

System (34) has two fixed points. The first fixed point $O_3 := (\rho, \eta) = (0, 0)$ has one unstable direction $(0,1)^T$ associated with the eigenvalue ξ and one center direction $(1,0)^T$ associated with the zero eigenvalue. The second fixed point is:

$$Q^6 := \quad (\rho, \eta) = (0, 1), \tag{35}$$

and it has one stable direction $(0,1)^T$ associated with the eigenvalue $-\xi$ and one center direction $(1,0)^T$ associated with the zero eigenvalue. The axis $\rho = 0$ is invariant, thus there exists an heteroclinic connection along the η-axis between the points O_3 and Q^6 that we denote by γ_3, see Figure 7(c).

Lemma 5.4 *There exists a unique center-unstable manifold $W^{c,u}$ at the point Q^6 that is smooth in α and that contains solutions that decay algebraically to Q^6 backwards in time. For $\alpha = \xi$ the set $H = 1$ coincides with $W^{c,u}$.*

Proof We rewrite the Hamiltonian (13b) in the (ρ, η) coordinates and then insert the condition $H = 1$ to obtain the implicit equation:

$$\frac{1}{\eta} - 1 + \mathrm{e}^{-\frac{1}{\rho}} \left(\frac{1}{\rho} + 1 + \frac{1}{\xi} \right) = 0. \tag{36}$$

Here $\rho \to 0$ gives $\eta \to 1$. Therefore Q^6 has a saddle-like behaviour with a unique center-unstable manifold $W^{c,u}$ that is tangent to $(1, 0)^T$ in Q^6. The invariant manifold $W^{c,u}$ is smooth in α and it maintains the center-unstable properties for small variation of α from $\alpha = \xi$. □

The orbit entering from chart κ_2 in the point $p_{3,\text{in}} := \kappa_{23}(p_{2,\text{out}}) = (\rho, \eta) = (\delta, 0)$ is connected through the stable and the unstable manifolds of O_3 to the point $p_{3,\text{out}}$ on $W^{c,u}$ with $\omega_3 = \delta$ as shown in Figure 7(c).

Remark 6 *We observe that the singularity at the origin of chart k_1 (26) has turned into three hyperbolic fixed points O_1, O_3 and Q^6 by using the blow-ups (27) and (33). After the blow-down we obtain the singular structure depicted in Figure 7(d).*

5.3. The reduced problem on $\mathcal{S}^{2,+}$

The previous analysis has described the phase space of (11) near infinity. In the following we analyse the interaction of the unbounded solutions of the reduced problem (11) with the fixed points $Q^{1,3,6,7}$ for variations of the parameter α. We follow the Melnikov-type approach of Chow et al. (1994), to describe how the closed orbits of the Hamiltonian system (12) break up near $\alpha = \xi$.
When $\alpha = \xi$ any bounded trajectory of (12) with $H = h$, $h \in (0, 1)$, intersects the y-axis in the two points D, d that correspond to the two real roots of the Lambert equation (15). We denote by D the root with $y > 0$ while we denote by d the one with $y < 0$, see Figure 8(a).
For $\alpha - \xi$ small, we compute the forward and backwards orbits $\gamma^+(t)$ and $\gamma^-(t)$ respectively emanating from D. The transversality condition (16) assures that $\gamma^+(t)$ and $\gamma^-(t)$ cross the y-axis for the first time in the points d^+ and d^- respectively.

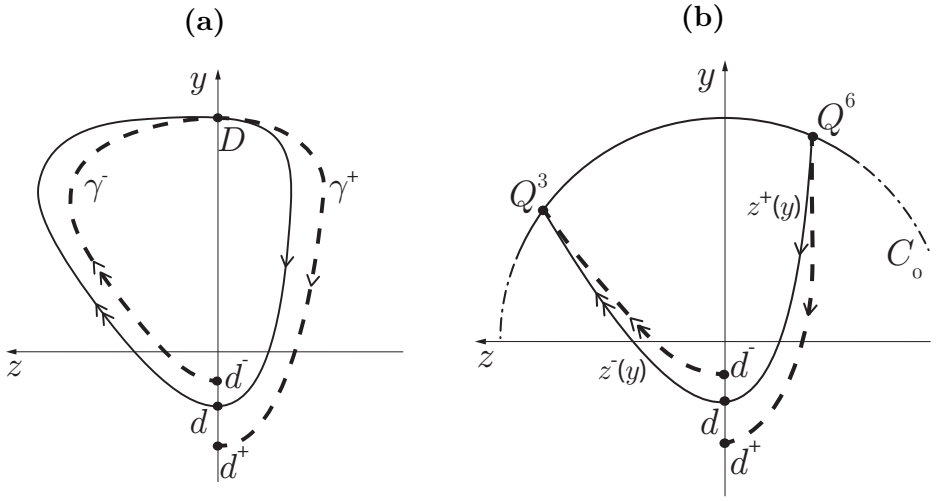

Figure 8: Perturbation of the Hamiltonian solutions for $\alpha - \xi$ small. In (a): closed orbit with $0 < H < 1$. In (b): heteroclinic connection for $H = 1$.

Hence we define the distance function:

$$\begin{aligned}\Delta(\alpha) &= H(d^+) - H(d^-),\\ &= \int_0^{T^+} \dot{H}(\gamma^+(t))\,\mathrm{d}t + \int_{T^-}^0 \dot{H}(\gamma^-(t))\,\mathrm{d}t,\\ &= \int_0^{T^+} \nabla H(h)\cdot f_0(y,z;\alpha)\,\mathrm{d}t + \int_{T^-}^0 \nabla H(h)\cdot f_0(y,z;\alpha)\,\mathrm{d}t,\end{aligned} \tag{37}$$

where $T^\pm = T^\pm(\alpha) \gtrless 0$ is the flow-time between D and d^+ and between D and d^- respectively. We Taylor expand (37) around $\alpha = \xi$:

$$\Delta(\alpha) = (\alpha - \xi)\Delta_\alpha(h) + \mathrm{O}((\alpha-\xi)^2), \tag{38}$$

with the quantity $\Delta_\alpha(h)$ defined as:

$$\begin{aligned}\Delta_\alpha(h) &= \int_{T_h^-}^{T_h^+} \nabla H(h)\cdot\frac{\partial f_0}{\partial\alpha}(y,z;\xi)\,\mathrm{d}t\\ &= \int_{T_h^-,}^{T_h^+} \xi \mathrm{e}^{-\xi y} z(\mathrm{e}^z - 1)\,\mathrm{d}t.\end{aligned} \tag{39}$$

In (39) we have denoted with $(y,z)(t)$ the solution of (12) for $H = h$ and $\alpha = \xi$. The times $T_h^\pm = T_h^\pm(\xi)$ are the forward and backwards times from D to d. The integrand

of (39) is always positive for $z \neq 0$ and therefore $\Delta_\alpha(h)$ is positive for any $h \in (0,1)$. We conclude from (38) that the forward flow $\gamma^+(t)$ spirals outwards for $\alpha > \xi$ while it spirals inwards for $\alpha < \xi$, in agreement with Figure 6.
We now extend the analysis above to the case of $H = 1$. In this case the points d^+ and d^- are the intersections of $W^{c,u}$ and $W^{c,s}$ with the y-axis respectively, see Figure 8(b). From the analysis above we know that $W^{c,s}$ and $W^{c,u}$ depend smoothly on α.

Lemma 5.5 *For $\alpha = \xi$ there is a unique heteroclinic connection between Q^3 and Q^6 on C_0. This connection is through the manifolds $W^{c,s}$ and $W^{c,u}$ and it corresponds to the set $H = 1$ in (13b). This set can be written as the union of two graphs $z = z^\pm(y)$ (see Figure 8(b)) with $y \geq -1/\xi$ so that $z^-(y)$ ($z^+(y)$ resp.) approaches Q^3 (Q^6) as $z^- = \mathrm{O}(y)$ ($z^+ = \mathrm{O}(\ln(y))$) for $y \to \infty$.*

Proof We rewrite the trajectory $H = 1$ as the graphs $z = z^\pm(y)$ for $y \geq -1/\xi$. The behaviour in forward time follows by considering the point $p_{1,\mathrm{in}}$ in condition (25) and blowing it down to the original variables (y, z). Similarly for the behaviour in backwards time by considering $p_{3,\mathrm{out}}$ in condition (36). □

Figure 6(b) follows from Lemma 5.5. When $\alpha = \xi$ the manifolds $W^{c,s}$ and $W^{c,u}$ cross the y-axis in the point $d := (y, z) = (-1/\xi, 0)$. We define the distance function $\Delta(\alpha)$ as in (37), we Taylor expand it around $\alpha = \xi$ as in (38) and we define $\Delta_\alpha(1)$ as in (39). Since the integrand of (39) is positive for $H = 1$ we just need to show that the improper integral (39) exists. From the reduced problem (11) we observe that $\dot{y} = \mathrm{e}^z - 1$, thus we rewrite (39) with respect to y as:

$$\Delta_\alpha(1) = \int_{-1/\xi}^{+\infty} \xi \mathrm{e}^{-\xi y} z^-(y)\, \mathrm{d}y - \int_{-1/\xi}^{+\infty} \xi \mathrm{e}^{-\xi y} z^+(y)\, \mathrm{d}y. \tag{40}$$

Recall from Lemma 5.5 that $z^-(y)$ is asymptotically linear in y for $y \to \infty$, while $z^+(y)$ decreases logarithmically with respect to y. The expression (40) therefore exists because of the exponential decay of the factor $\exp(-\xi y)$ and furthermore it is positive. We remark that $\Delta_\alpha(h)$ in (39) converges to $\Delta_\alpha(1)$ for $h \to 1$, since the orbit segment on $C_{0,\infty}$ does not give any contribution to (40).

Now we finish the proof of Proposition 5.2 by considering α as in (21). When $\alpha < \xi$ the set $W^{c,u}$ contracts towards the origin, because $\Delta(\alpha) < 0$ in (38). Furthermore the set $W^{c,s}$ is backwards asymptotic to Q^7 and acts as a separator

between the basin of attraction of the origin and the basin of attraction of Q^1. A similar argument covers the case $\alpha > \xi$. This concludes the proof of Proposition 5.2 and justifies Figures 6(a) and 6(c). Hence we have established that no periodic orbit exists on C_0 for $\alpha > \xi$ and $\varepsilon = 0$. In section 6 we show that for $\varepsilon \ll 1$ there is only one periodic orbit that persists on the slow manifold given $\alpha - \xi = \mathrm{O}(\varepsilon)$.

6. Analysis of the perturbed problem for $\varepsilon > 0$

Consider the original problem (1) and $0 < \mu < 1$ small but fixed. Then the compact manifold:

$$S_0 = \{(x, y, z) \in C_0 | \quad 0 \leq H(y, z) \leq 1 - \mu\}, \tag{41}$$

is normally hyperbolic for $\varepsilon = 0$. Therefore Fenichel's theory guarantees that for ε sufficiently small there exists a locally invariant manifold S_ε that is $\mathrm{O}(\varepsilon)$-close to S_0 and is diffeomorphic to it. Moreover the flow on S_ε converges to the flow of the reduced problem (11) for $\varepsilon \to 0$. A computation shows that S_ε at first order is:

$$z = -(x + \xi y) + \varepsilon\xi \mathrm{e}^{-2(x+\xi y)} \left(\alpha(x + \xi y) + \xi(y + 1) - \xi \mathrm{e}^{x+\xi y}\right) + \mathrm{O}(\varepsilon^2),$$

hence we have the following vector field $f_\varepsilon(y, z; \alpha, \varepsilon)$ on S_ε:

$$f_\varepsilon(y, z; \alpha, \varepsilon) := \begin{cases} \dot{y} &= \mathrm{e}^z - 1 - \varepsilon\xi\chi\mathrm{e}^{2z} + \mathrm{O}(\varepsilon^2), \\ \dot{z} &= \chi - \varepsilon\xi\chi\mathrm{e}^{2z}(\alpha z - \xi y + \alpha - \xi + 1) + \mathrm{O}(\varepsilon^2), \end{cases} \tag{42}$$

with $\chi(y, z) = \alpha z\mathrm{e}^z - \xi y\mathrm{e}^z - \xi\mathrm{e}^z + \xi$.

Proposition 6.1 *Consider the compact manifold S_0 defined in (41). Then S_0 perturbs to a locally invariant slow manifold S_ε for $\varepsilon \ll 1$. On S_ε the origin of (42) undergoes a supercritical Hopf bifurcation for:*

$$\alpha = \alpha_H := \xi - \varepsilon\xi^2 + \mathrm{O}(\varepsilon^2), \tag{43}$$

with the first Lyapunov coefficient:

$$a = -\frac{1}{8}\varepsilon\xi^3(1 + \xi) + \mathrm{O}(\varepsilon^2) < 0. \tag{44}$$

Therefore for $\alpha \in (\alpha_H, \alpha_H + c(\mu)\varepsilon)$ with $c(\mu)$ sufficiently small, there exists a family of locally unique attracting limit cycles with amplitude of order $\mathrm{O}\left(\sqrt{-(\alpha - \alpha_H)/a}\right)$.

The proof of Proposition 6.1 follows from straightforward computations. We remark that since (44) is proportional to ε, it follows that the results of Proposition 6.1 are valid only for a very small interval of α around α_H. We use the analysis of section 5.3 to extend the small limit cycles of Proposition 6.1 into larger ones.

Proposition 6.2 *Consider the slow manifold S_ε of Proposition 6.1. On S_ε there exists a family of closed periodic orbits for*

$$\alpha = \alpha_M(h) := \xi - \varepsilon \frac{\Delta_\varepsilon(h)}{\Delta_\alpha(h)} + \mathrm{O}(\varepsilon^2), \tag{45}$$

where $h \in [c_1(\mu), 1 - c_2(\mu)]$ with $(c_1, c_2)(\mu)$ small. The quantity $\Delta_\varepsilon(h)$ is defined as:

$$\Delta_\varepsilon(h) = \int_{T_h^-}^{T_h^+} \nabla H(h) \cdot \frac{\partial f_\varepsilon}{\partial \varepsilon}(y, z; \xi, 0)\, \mathrm{d}t, \tag{46}$$

while $\Delta_\alpha(h) > 0$ was defined in (39).

Proof By Fenichel's theorem we know that the flow on S_ε converges to the flow of the reduced problem (11) for $\varepsilon \to 0$. Therefore we can define the distance function $\Delta(\alpha, \varepsilon)$ similarly to (37) whose Taylor expansion around $\alpha = \xi$ and $\varepsilon = 0$ is:

$$\Delta(\alpha, \varepsilon) = (\alpha - \xi)\Delta_\alpha(h) + \varepsilon \Delta_\varepsilon(h) + \mathrm{O}((\alpha - \xi + \varepsilon)^2), \tag{47}$$

with $\Delta_\alpha(h)$ and $\Delta_\varepsilon(h)$ defined in (39) and (46) respectively. The integrand of $\Delta_\alpha(h)$ is strictly positive for all $h \in (0, 1)$, therefore we can apply the implicit function theorem to (47) for $\Delta(\alpha, \varepsilon) = 0$ and obtain the result (45). □

In Figure 9 we show a numerical computation of the leading order coefficient in (45) for an interval of energies $H = h \in (0, 0.6]$. No saddle-node bifurcations occur in this interval. We expect a similar behaviour for larger values of h but we did not manage to compute this due to the intrinsic slow-fast structure of the reduced problem. It might be possible to study the term $\Delta_\varepsilon(h)/\Delta_\alpha(h)$ analytically by using the results of Lemma 5.5 but the expressions are lengthy and we did not find an easy way.
The analysis above can only explain the limit cycles that appear for $\alpha - \xi = \mathrm{O}(\varepsilon)$ and it does not justify the limit cycles of Figure 1 that appear for larger values of $\alpha - \xi$. For this reason we proceed to study the full problem (1) at infinity, introducing its compactification through the Poincaré sphere.

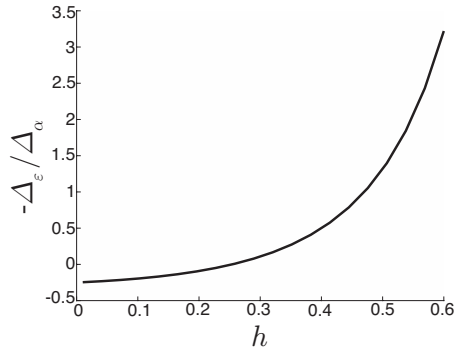

Figure 9: Plot of the leading order coefficient in (45) for $\xi = 0.5$ and $h \in (0, 0.6]$.

7. Statement of the main result

In this section we find a connection at infinity between the points Q^1 and Q^6 that will establish a return mechanism to C_0 of the unbounded solutions of (4) when $\varepsilon = 0$ and $\alpha > \xi$. This mechanism will be the foundation for the existence of limit cycles when $0 < \varepsilon \ll 1$ and $\alpha - \xi \geq c > 0$.
Similar to section 5, we introduce a four-dimensional Poincaré sphere $\mathcal{S}^{3,+}$:

$$\mathcal{S}^{3,+} := \left\{(X, Y, Z, W) \in \mathbb{R}^4 \middle| \quad X^2 + Y^2 + Z^2 + W^2 = 1, \quad W \geq 0\right\}. \tag{48}$$

The fast problem (4) is interpreted as a directional chart K_2 on $\mathcal{S}^{3,+}$ defined for $W = 1$:

$$K_2 := \mathcal{S}^{3,+} \cap \{W = 1\}, \quad x_2 = \frac{X}{W}, y_2 = \frac{Y}{W}, z_2 = \frac{Z}{W},$$

therefore the vector field in chart K_2 is obtained by introducing the subscript in (4):

$$\begin{aligned} \dot{x}_2 &= -\varepsilon \mathrm{e}^{z_2}(x_2 + (1+\alpha)z_2), \\ \dot{y}_2 &= \varepsilon\left(\mathrm{e}^{z_2} - 1\right), \\ \dot{z}_2 &= -\mathrm{e}^{-z_2}\left(y_2 + \frac{x_2 + z_2}{\xi}\right). \end{aligned} \tag{49}$$

The points at infinity in K_2 correspond to $W = 0$ which is a sphere S^2. We introduce the two directional charts:

$$K_3 := \mathcal{S}^{3,+} \cap \{Z = 1\}, \quad x_3 = \frac{X}{Z}, y_3 = \frac{Y}{Z}, w_3 = \frac{W}{Z}, \tag{50a}$$

$$K_1 := \mathcal{S}^{3,+} \cap \{Y = 1\}, \quad x_1 = \frac{X}{Y}, z_1 = \frac{Z}{Y}, w_1 = \frac{W}{Y}. \tag{50b}$$

We have the following transformations between the charts:

$$K_{23}: \quad w_3 = z_2^{-1}, \quad x_3 = x_2 z_2^{-1}, \quad y_3 = y_2 z_2^{-1}, \tag{51a}$$

$$K_{21}: \quad w_1 = y_2^{-1}, \quad x_1 = x_2 y_2^{-1}, \quad z_1 = z_2 y_2^{-1}, \tag{51b}$$

$$K_{31}: \quad w_1 = w_3 y_3^{-1}, \; x_1 = x_3 y_3^{-1}, \quad z_1 = y_3^{-1}, \tag{51c}$$

that are defined for $z_2 > 0$, $y_2 > 0$ and $y_3 > 0$ respectively. The inverse transformations are defined similarly. The three points $Q^1, Q^3 \in K_3$ and $Q^6 \in K_1$:

$$Q^1 := \quad (x_3, y_3, w_3) = (-1, 0, 0), \tag{52a}$$

$$Q^3 := \quad (x_3, y_3, w_3) = \left(-1-\alpha, \frac{\alpha}{\xi}, 0\right), \tag{52b}$$

$$Q^6 := \quad (x_1, z_1, w_1) = (-\xi, 0, 0), \tag{52c}$$

introduced in Proposition 5.1 and the three points $Q^2, Q^4 \in K_3$ and $Q^5 \in K_1$:

$$Q^2 := \quad (x_3, y_3, w_3) = (-1-\alpha, 0, 0), \tag{53a}$$

$$Q^4 := \quad (x_3, y_3, w_3) = \left(-1-\alpha, \frac{2\alpha}{\xi}, 0\right), \tag{53b}$$

$$Q^5 := \quad (x_1, z_1, w_1) = \left(-\frac{\xi}{2\alpha}(1+\alpha), \frac{\xi}{2\alpha}(1-\alpha), 0\right), \tag{53c}$$

are going to play a role in the following, together with the lines:

$$L_0 := \quad \{(x_3, y_3, w_3) | \quad x_3 + 1 + \alpha = 0, \; w_3 = 0\}, \tag{54a}$$

$$C_{0,\infty} := \quad \{(x_3, y_3, w_3) | \quad x_3 + \xi y_3 + 1 = 0, \; w_3 = 0\}. \tag{54b}$$

Notice that the line L_0 corresponds to the intersection of the family of nullclines (10) with infinity through the transformation K_{23}. Our main result is the following conjecture:

Conjecture 7.1 *Fix $\alpha > \xi$. Then for $0 < \varepsilon \ll 1$ there exists an attracting limit cycle Γ_ε that converges to the* singular cycle Γ_0*, where Γ_0 consists of the points $Q^{1,2,4,5,6}$ and of the union of the following sets:*

- *$\gamma^{1,2}$ connecting Q^1 with Q^2. In chart K_3 the segment $\gamma^{1,2}$ is:*

$$\gamma^{1,2} := \{(x_3, y_3, w_3) \in K_3 | \quad x_3 \in (-1-\alpha, -1), y_3 = 0, w_3 = 0\}. \tag{55}$$

- $\gamma^{2,4}$ *connecting* Q^2 *with* Q^4 *along* L_0. *In chart* K_3 *the segment* $\gamma^{2,4}$ *is:*

$$\gamma^{2,4} := \left\{ (x_3, y_3, w_3) \in K_3 | \quad x_3 = -1-\alpha, y_3 \in \left(0, \frac{2\alpha}{\xi}\right), w_3 = 0 \right\}. \tag{56}$$

- $\gamma^{4,5}$ *connecting* Q^4 *with* Q^5. *This segment is a fast fiber of* (6) *and in chart* K_1 *the segment* $\gamma^{4,5}$ *is:*

$$\gamma^{4,5} := \left\{ (x_1, z_1, w_1) \in K_1 | \quad x_1 = -\frac{\xi}{2\alpha}(1+\alpha), z_1 \in \left(\frac{\xi}{2\alpha}(1-\alpha), \frac{\xi}{2\alpha}\right), w_1 = 0 \right\}. \tag{57}$$

- $\gamma^{5,6}$ *connecting* Q^5 *with* Q^6 *on* $C_{0,\infty}$. *In chart* K_1 *the segment* $\gamma^{5,6}$ *is:*

$$\gamma^{5,6} := \left\{ (x_1, z_1, w_1) \in K_1 | \quad x_1 = -\xi - z_1, z_1 \in \left(0, \frac{\xi}{2\alpha}(1-\alpha)\right), w_1 = 0 \right\}. \tag{58}$$

- $W^{c,u}$ *connecting* Q^6 *with* Q^1 *on the critical manifold* C_0.

Figure 10 gives a representation of Γ_0 and of its different segments. Figure 10(a) shows the complete orbit while figures 10(b) and 10(c) show the portions of Γ_0 that are visible along the charts K_3 and K_1 respectively. We provide the foundations of a rigorous proof of Conjecture 7.1 in the next section.

Remark 7 *Here we collect the results of sections 6 and 7. When* $\varepsilon = 0$ *and* $\alpha = \xi$ *then there exists a family of periodic solutions on* $\mathcal{S}^{3,+}$, *corresponding to the Hamiltonian orbits with* $H \in (0,1)$. *For* $\alpha > \xi$ *only the cycle* Γ_0 *exists. When* $0 < \varepsilon \ll 1$ *and* $\alpha - \xi = \mathrm{O}(\varepsilon)$ *then there exists a limit cycle resembling the bounded Hamiltonian orbits. For larger values of* $\alpha - \xi$ *we conjecture that the limit cycle tends to* Γ_0. *Figure 11 shows the conjectured bifurcation diagram of the periodic orbits.*

In Figure 12 we show some numerical simulations that support Conjecture 7.1. Figure 12(a) illustrates the limit cycles Γ_ε for three different values of $\varepsilon \in \{10^{-8}, 10^{-4}, 10^{-2}\}$ with $\alpha = 0.9$ and $\xi = 0.5$ while Figures 12(b), 12(c) show the portions of Γ_ε that appear in the two charts K_3 and K_1 respectively.
We notice that the amplitude of the orbits increases for decreasing values of the parameter ε and that both the plane C_0 and the line L_0 play an important role. Close to the origin the dynamics evolves on the critical manifold while sufficiently far from the origin C_0 loses the normal hyperbolicity and the line L_0 becomes relevant. Indeed in Figure 12(b) we see that the solutions contract towards L_0 following $\gamma^{1,2}$ and then evolve with increasing values of y_3 following $\gamma^{2,4}$. When the solutions are close to Q^4 they follow $\gamma^{4,5}$ and contract again towards C_0 along a direction that tends to the fast fiber for $\varepsilon \to 0$, as we can see in Figure 12(c).

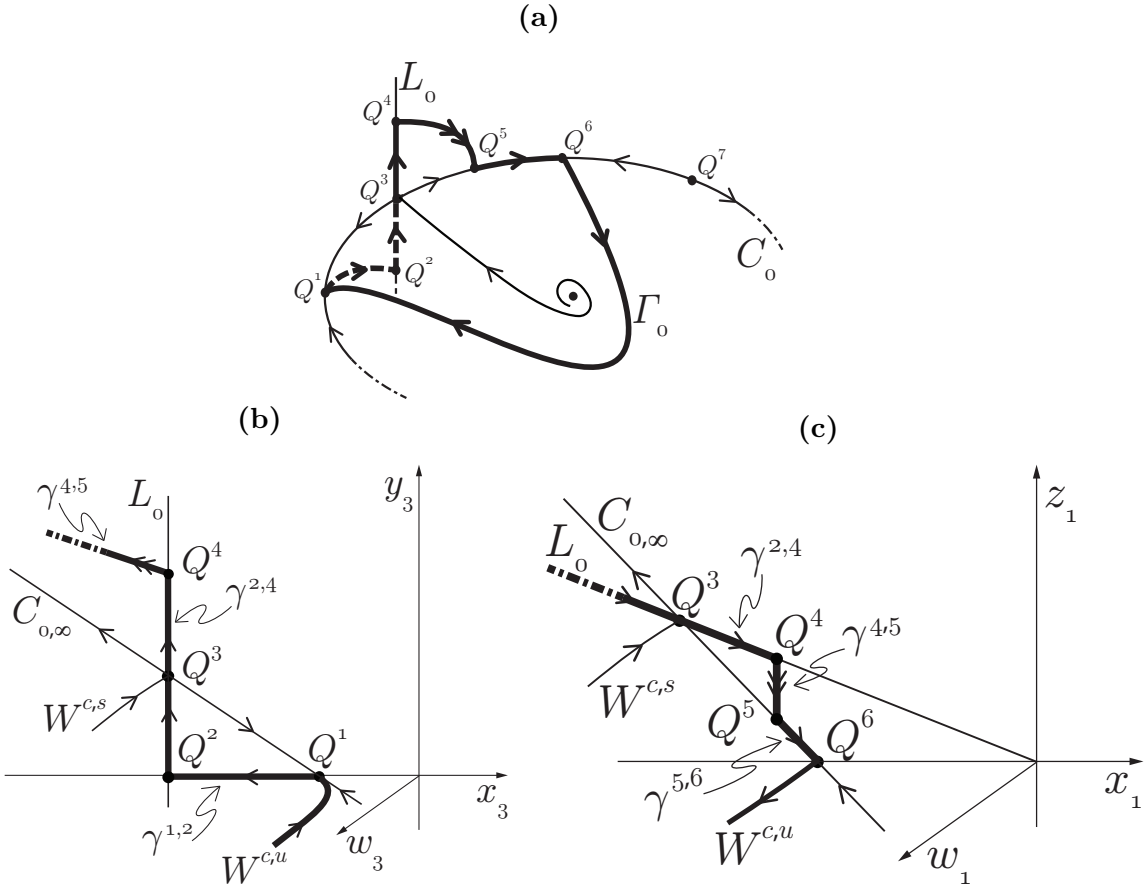

Figure 10: Schematisation of Γ_0 in (a). The segment $\gamma^{1,2}$ is visible only in chart K_3, see (b). The segment $\gamma^{5,6}$ is visible only in chart K_1, see (c). The remaining segments $\gamma^{2,4}$, $\gamma^{4,5}$ are visible in both charts.

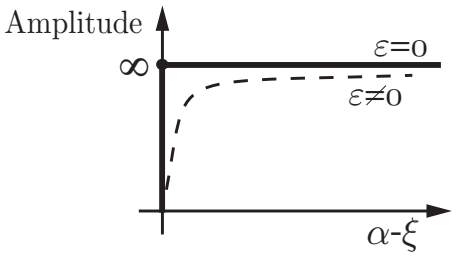

Figure 11: Conjectured bifurcation diagram of the limit cycles for $\varepsilon \ll 1$.

8. Sketch of the proof

We lay out the foundations of a rigorous proof of Conjecture 7.1 by identifying the singular structure of Γ_0 through a series of blow-ups. In particular we study the dynamics of (4) along the two directional charts K_3 and K_1 respectively. We leave the full details of the proof for $0 < \varepsilon \ll 1$ to another manuscript.

8.1. Chart K_3

We obtain the vector field in chart K_3 by inserting condition (50a) into the fast problem (49). This vector field is de-singularized at $w_3 = 0$ by division of e^{1/w_3}. For the sake of readability we drop the subscripts:

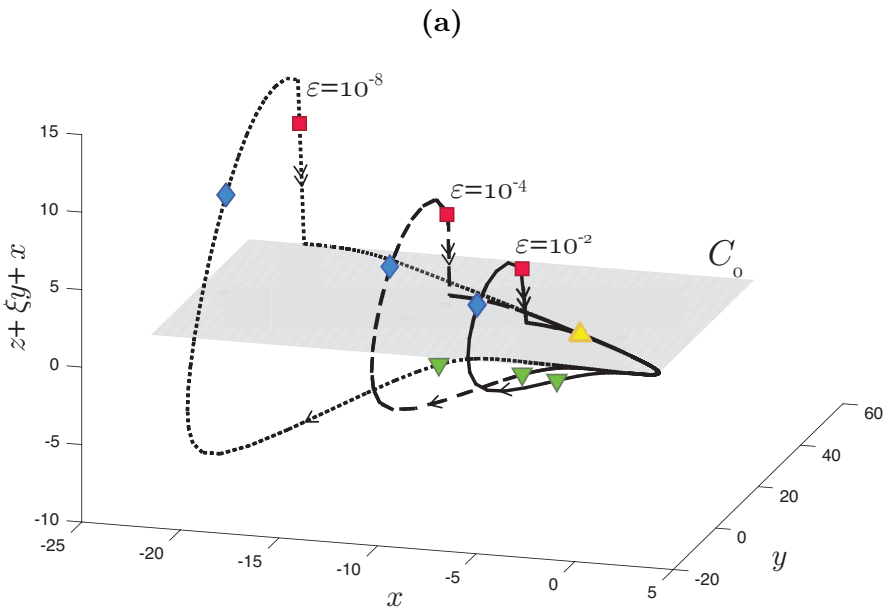

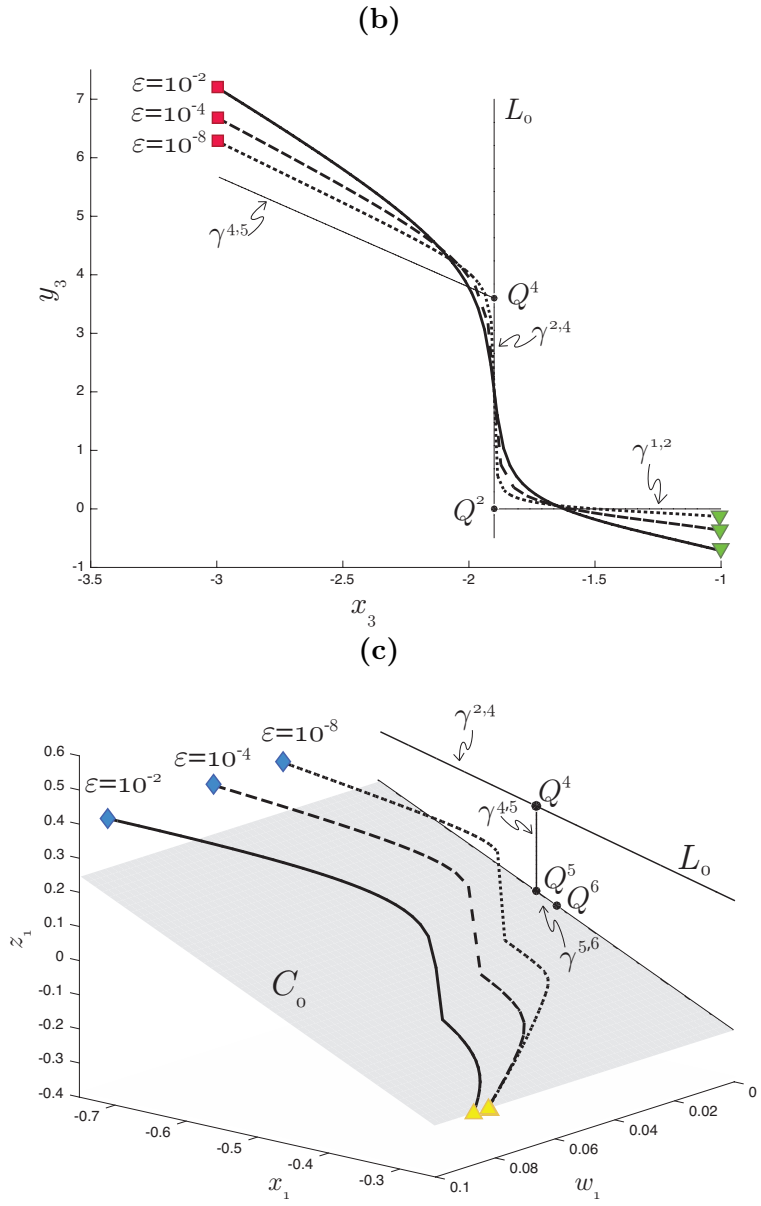

Figure 12: Figure (a): numerical simulation of (1) for $\varepsilon \in \{10^{-8}, 10^{-4}, 10^{-2}\}$, $\alpha = 0.9$ and $\xi = 0.5$. In (b) we illustrate the portion of Γ_ε visible in chart K_3, i.e. between the green lower triangle and the red square. In (c) we show the portion of Γ_ε visible in K_1, i.e. between the blue diamond and the yellow upper triangle. We remark that the portion between the blue triangle and the red square is visible in both the charts K_3 and K_1 since the two charts overlap for $y_3 > 0$ or $z_1 > 0$. Colours are available in the online version.

$$
\begin{aligned}
\dot{w} &= w\mathrm{e}^{-\frac{2}{w}}\left(y+\frac{x+1}{\xi}\right),\\
\dot{x} &= -\varepsilon(x+1+\alpha)+x\mathrm{e}^{-\frac{2}{w}}\left(y+\frac{x+1}{\xi}\right),\\
\dot{y} &= \varepsilon w(1-\mathrm{e}^{-\frac{1}{w}})+y\mathrm{e}^{-\frac{2}{w}}\left(y+\frac{x+1}{\xi}\right),\\
\dot{\varepsilon} &= 0.
\end{aligned}
\tag{59}
$$

System (59) is a four-dimensional vector field defined on $\mathbb{R}^4$ where we treat the parameter ε as a variable. The set $w=\varepsilon=0$ consists of non-hyperbolic fixed points of (59) and the two lines $C_{0,\infty}$ and L_0 (54) are contained within this set. Since we consider a regime of w sufficiently small, we approximate $1-\mathrm{e}^{-1/w}\simeq 1$ in the y-term of (59) to simplify the computations. Qualitatively this has no effects on the results. Now we briefly outline the following analysis of chart K_3, whose results are portrayed in Figure 10(b). First we blow-up the vector field (59) around Q^1 in order to extend the hyperbolicity of C_0 up to infinity. To do so we need to get rid of the exponential terms. We deal with it by introducing a new variable q:

$$
q=\mathrm{e}^{-\frac{2}{w}},
\tag{60}
$$

so that the extended system contains only algebraic terms in its variables. Indeed by differentiating (60) with respect to time we obtain:

$$
\begin{aligned}
\dot{q} &= 2w^{-2}\dot{w}\mathrm{e}^{-\frac{2}{w}},\\
&= 2w^{-1}q\left(y+\frac{x+1}{\xi}\right),
\end{aligned}
\tag{61}
$$

where we have used (59) and (60). Inserting (61) into (59) we obtain the five-dimensional vector field:

$$\begin{aligned}
\dot{w} &= w^2 q \left(y + \frac{x+1}{\xi} \right), \\
\dot{x} &= -\varepsilon w (x + 1 + \alpha) + xqw \left(y + \frac{x+1}{\xi} \right), \\
\dot{y} &= \varepsilon w^2 + yqw \left(y + \frac{x+1}{\xi} \right), \\
\dot{q} &= 2q^2 \left(y + \frac{x+1}{\xi} \right), \\
\dot{\varepsilon} &= 0.
\end{aligned} \tag{62}$$

after multiplying the right hand side by w. The evolution of q in (62) is slaved by w through (60). However, this dependence is not explicit and we will refer to it only when needed. We refer to (Kristiansen 2016) for further details on this approach. Using repeated blow-ups, different charts and hyperbolic methods we then establish a connection $\gamma^{1,2}$ from the point Q^1 to the point $Q^2 \in L_0$. Thereafter we study the dynamics along L_0 by doing an additional blow-up. This will establish the connection $\gamma^{2,4}$ from Q^2 to Q^4 on L_0. We will continue the rest of the analysis – corresponding to the identification of the trajectories $\gamma^{4,5}$ and $\gamma^{5,6}$ – in chart K_1. We refer the reader to section 8.2 for the continuation of the analysis from the point Q^4.

System (62) has a 3-dimensional space of non-hyperbolic fixed points for $\varepsilon = q = 0$, since each point has a quintuple zero eigenvalue. To overcome the degeneracy we first introduce the blow-up map:

$$q = \bar{r}\bar{q}, \quad \varepsilon = \bar{r}\bar{\epsilon}, \tag{63}$$

with $(\bar{q}, \bar{\epsilon}) \in S^1$ and $\bar{r} \geq 0$. The variables $(w, x, y) \in \mathbb{R}^3$ in (62) are kept unchanged so that the set $q = \varepsilon = 0$ is blown-up to a cylinder $\mathbb{R}^3 \times S^1$. We remark that the quantity ε in (63) is a constant, hence the blown-up space is foliated. We restrict our analysis to the two local charts:

$$\mathcal{K}_1 : \quad q = r_1, \qquad \varepsilon = r_1 \epsilon_1, \tag{64a}$$

$$\mathcal{K}_2 : \quad q = r_2 q_2, \qquad \varepsilon = r_2. \tag{64b}$$

Notice that $q_2 = \mathrm{O}(1)$ in chart $\mathcal{K}_2$ corresponds through (60) to $w = \mathrm{O}(\ln^{-1} \varepsilon^{-1})$ or $z_2 = \mathrm{O}(\ln \varepsilon^{-1})$. This regime is relevant for the naïve identification of L_0 in (9).

Chart $\mathcal{K}_1$ To simplify the following analysis we place the x-axis on C_0 by introducing the new coordinate:

$$\tilde{x} = x + \xi y + 1, \tag{65}$$

so that the point Q^1 is centered in the origin of chart K_3. We insert the transformation (64a) into (62) and divide out a common factor of r_1 to obtain the de-singularized system in chart $\mathcal{K}_1$. For the sake of readability we drop the subscript and the tilde henceforth:

$$\begin{aligned}
\dot{w} &= w^2 \frac{x}{\xi}, \\
\dot{x} &= -\epsilon w(\alpha + x) - w(1-x)\frac{x}{\xi} + \epsilon w \xi (w + y), \\
\dot{y} &= \epsilon w^2 + y w \frac{x}{\xi}, \\
\dot{r} &= 2r \frac{x}{\xi}, \\
\dot{\epsilon} &= -2\epsilon \frac{x}{\xi}.
\end{aligned} \tag{66}$$

In (66) the variables (w, x, y, ϵ) are independent of r, therefore we can directly reduce the dimension of the system. The origin of the reduced chart $\mathcal{K}_1$ is still degenerate since it has a quadruple zero eigenvalue. To overcome the degeneracy we introduce the following blow-up of $C_{0,\infty}$:

$$w = \bar{r}\bar{w}, \quad x = \bar{r}\bar{x}, \quad \epsilon = \bar{r}\bar{\epsilon}, \tag{67}$$

where $(\bar{w}, \bar{x}, \bar{\epsilon}) \in S^2$ and $\bar{r} \geq 0$ small. The variable $y \in \mathbb{R}$ is kept unchanged. We project the blown-up dynamics onto the following local charts:

$$\mathtt{K}_1 : \quad w = r_1, \qquad x = r_1 x_1, \qquad \epsilon = r_1 \epsilon_1, \tag{68a}$$

$$\mathtt{K}_2 : \quad w = r_2 w_2, \quad x = r_2 x_2 \qquad \epsilon = r_2. \tag{68b}$$

Chart $\mathtt{K}_1$ We insert (68a) into system (66) and divide the vector field by the common divisor r_1 to obtain the de-singularized dynamics:

$$\begin{aligned}
\dot{r}_1 &= r_1^2 \frac{x_1}{\xi}, \\
\dot{x}_1 &= -\frac{x_1}{\xi} - \epsilon_1(\alpha + r_1 x_1 - \xi(r_1 + y)), \\
\dot{y} &= y r_1 \frac{x_1}{\xi} + \epsilon_1 r_1^2, \\
\dot{\epsilon}_1 &= -\epsilon_1 \frac{x_1}{\xi}(2 + r_1).
\end{aligned} \tag{69}$$

Now we notice that the line $r_1 = 0, x_1 = 0, \epsilon_1 = 0$ has gained hyperbolicity. We therefore obtain the following:

Lemma 8.1 *Let $\epsilon_1 < \delta$ with $\delta > 0$ fixed. Then in (69) there exists an attracting 3-dimensional center manifold:*

$$x_1 = -\epsilon_1(\alpha\xi + \mathrm{O}(\epsilon_1)). \tag{70}$$

For the level sets $\varepsilon = const.$ and $q = \mathrm{e}^{-2/w}$, the center manifold (70) is the extension of the slow-manifold S_ε introduced in Proposition 6.1 into chart $\mathtt{K}_1$.

As a consequence of Lemma 8.1 we have extended the hyperbolicity of C_0 up to $C_{0,\infty}$ for $\epsilon_1 = 0$. The dynamics within (70) is obtained by substituting (70) into (69) and by dividing the resulting vector field by ϵ_1:

$$\begin{aligned}
\dot{r}_1 &= -\alpha r_1^2 \left(1 + \mathrm{O}(\epsilon_1)\right), \\
\dot{y} &= r_1(r_1 - y\alpha) \left(1 + \mathrm{O}(\epsilon_1)\right), \\
\dot{\epsilon}_1 &= \alpha\epsilon_1 \left(1 + \mathrm{O}(r_1 + \epsilon_1)\right).
\end{aligned} \tag{71}$$

System (71) has two invariant planes for $r_1 = 0$ and $\epsilon_1 = 0$ and the dynamics along them is shown in Figure 13. All the trajectories on the plane $\epsilon_1 = 0$ contract towards the origin which corresponds to the point Q^1. The plane $r_1 = 0$ is foliated with invariant lines where y is fixed and along these lines the variable ϵ_1 grows exponentially. We set:

$$P_{1,\mathrm{out}} := \quad (r_1, x_1, y, \epsilon_1) = (0, -\delta(\alpha\xi + \mathrm{O}(\delta)), 0, \delta), \tag{72}$$

belonging to (70) and $y = 0$. We continue the point $P_{1,\mathrm{out}}$ using chart $\mathtt{K}_2$.

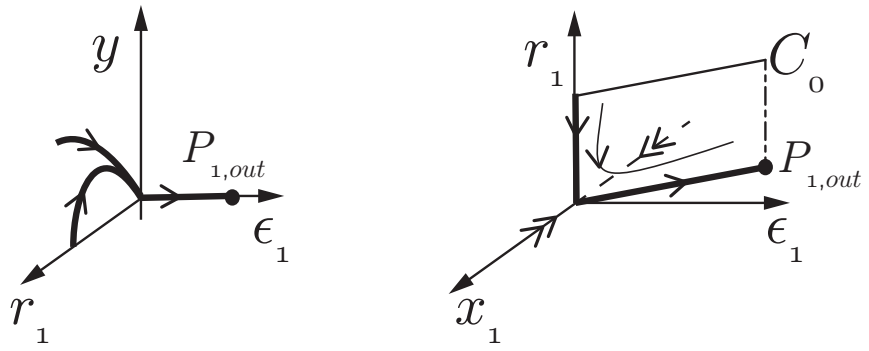

Figure 13: Dynamics within (70) projected along (r_1, y, ϵ_1) on the left and along (x_1, r_1, ϵ_1) on the right.

Chart $\mathtt{K}_2$ The dynamics on $\mathtt{K}_2$ is obtained by substituting condition (68b) into (66) and by dividing the right hand side by the common divisor r_2:

$$\begin{aligned}
\dot{r}_2 &= -2r_2\frac{x_2}{\xi},\\
\dot{w}_2 &= w_2\frac{x_2}{\xi}(2 + r_2w_2),\\
\dot{x}_2 &= 2\frac{x_2^2}{\xi} - w_2(\alpha + r_2x_2) + w_2\frac{x_2}{\xi}(r_2x_2 - 1) + w_2\xi(r_2w_2 + y),\\
\dot{y} &= r_2^2w_2^2 + yr_2w_2\frac{x_2}{\xi}.
\end{aligned} \tag{73}$$

This system has a fixed point in the origin with four zero eigenvalues. Therefore we introduce the blow-up map:

$$w_2 = \rho^2, \quad x_2 = -\rho x. \tag{74}$$

We substitute (74) in (73), drop the subscript and divide by the common divisor ρ to obtain the de-singularized vector field:

$$\begin{aligned}
\dot{r} &= 2r\frac{x}{\xi},\\
\dot{\rho} &= -\frac{\rho x}{2\xi}(2 + r\rho^2),\\
\dot{x} &= \alpha - r\rho x - \rho\frac{x}{\xi}(1 + r\rho x) - \xi(r\rho^2 + y) - \frac{x^2}{\xi} + r\frac{\rho^2x^2}{2\xi},\\
\dot{y} &= r^2\rho^3 - yr\rho^2\frac{x}{\xi}.
\end{aligned} \tag{75}$$

Lemma 8.2 *The point $P_{1,out}$ in (72) is translated in chart $\mathtt{K}_2$ to the point $P_{2,in} = \mathtt{K}_{12}(P_{1,out})$, where:*

$$P_{2,in} := \quad (r, \rho, x, y) = (0, \delta^{-1/2}, \alpha\xi, 0). \tag{76}$$

The solution with initial condition in $P_{2,in}$ converges towards the stable node:

$$P_{2,out} := \quad (r, \rho, x, y) = (0, 0, \sqrt{\alpha\xi}, 0), \tag{77}$$

on the invariant plane $r = 0$, see Figure 14.

Proof We first rewrite system (75) as a parameter independent system for $r = 0$. For this reason we introduce the new variables (x_1, ρ_1, t_1) such that $x = \sqrt{\alpha\xi}x_1, \rho = \sqrt{\alpha\xi}\rho_1, \tilde{t}_2 = \sqrt{\xi/\alpha}t_1$ and where $\tilde{t}_2$ is the time in equation (75). We drop the subscript henceforth and for $r = 0$ we get the non-trivial dynamics:

$$\begin{aligned} \dot{\rho} &= -\rho x, \\ \dot{x} &= 1 - \rho x - x^2, \end{aligned} \tag{78}$$

with the dot meaning the time derivative with respect to t_1. System (78) has a stable node in:

$$(\rho, x) = (0, 1). \tag{79}$$

Moreover the region $\rho \geq 0, x \geq 0$ is invariant and $P_{2,\text{in}}$ lies inside this region. In particular the point $P_{2,\text{in}}$ is contained in the trapping region $T_r := \{x \geq 0\} \cap \{\rho \geq 0\} \cap \{x \leq 2\} \cap \{\rho \leq \delta^{-1}\}$ and the node (79) is the only equilibrium inside T_r. At the boundaries of T_r the vector field points everywhere inwards the region itself, see Figure 14. Moreover a direct analysis of the nullclines of (78) excludes the presence of limit cycles in T_r. We conclude that the solution departing from $P_{2,\text{in}}$ must be forward asymptotic to $(\rho, x) = (0, 1)$, that in the original coordinates corresponds to $P_{2,\text{out}}$ (77). □

We continue the analysis by following the unstable manifold of the fixed point (77) on the invariant plane $\rho = 0$. We denote this new trajectory by γ_2^1 such that:

$$\gamma_2^1 := \left\{ (r, \rho, x, y) \in \mathbb{R}^{2,+} \times \mathbb{R}^2 | \quad r \geq 0, \rho = 0, x = \sqrt{\alpha\xi}, y = 0 \right\}. \tag{80}$$

On the blown-down charts $\mathtt{K}_2$ and $\mathcal{K}_1$, the trajectory γ_2^1 keeps its invariant properties. Therefore for large values of r we follow γ_2^1 in chart $\mathcal{K}_2$ as defined in (64b). We remark that all the dynamics that we have described so far is taking place at the point Q^1.

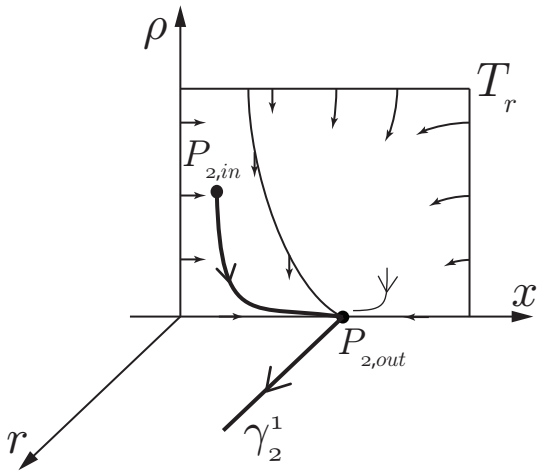

Figure 14: Dynamics in chart $\mathtt{K}_2$. The trapping region T_r is defined on the plane $r = 0$.

Chart $\mathcal{K}_2$ We substitute condition (64b) into (62) and divide the right-hand side by the common divisor r_2 to obtain the de-singularized dynamics in chart $\mathcal{K}_2$.

$$\begin{aligned}
\dot{w} &= w^2 q_2 \left(y + \frac{x+1}{\xi} \right), \\
\dot{x} &= -w(x+1+\alpha) + xwq_2 \left(y + \frac{x+1}{\xi} \right), \\
\dot{y} &= w^2 + ywq_2 \left(y + \frac{x+1}{\xi} \right), \\
\dot{q_2} &= 2q_2^2 \left(y + \frac{x+1}{\xi} \right), \\
\dot{r_2} &= 0.
\end{aligned} \tag{81}$$

Notice that to describe the equations of $\mathcal{K}_2$ in (81) we use the old variable x and not $\tilde{x}$ as we have done in chart $\mathcal{K}_1$. The relation between x and $\tilde{x}$ is defined in (65). We reduce the following analysis to the four variables (w, x, y, q_2) since they are independent of r_2. The trajectory γ_2^1 is transformed into chart $\mathcal{K}_2$ as:

$$\mathcal{K}_{12}(\gamma_2^1) := \left\{ (w, x, y, q_2) \in \mathbb{R}^+ \times \mathbb{R}^3 | \quad w = 0, x = -1, y = 0, q_2 \geq 0 \right\}, \tag{82}$$

using (68) and contracts towards the fixed point:

$$(w, x, y, q_2) = (0, -1, 0, 0), \tag{83}$$

as follows from (80). For $w = q_2 = 0$ we have that system (81) is a plane of non-hyperbolic fixed points. To overcome the loss of hyperbolicity we introduce the following blow-up map after having dropped the subscript:

$$w = \bar{r}\bar{w}, \quad q = \bar{r}\bar{q}, \tag{84}$$

where $(\bar{w}, \bar{q}) \in S^1$ and $\bar{r} \geq 0$. We restrict our analysis to the two charts:

$$\hat{\mathtt{K}}_1 : \quad w = r_1, \qquad q = r_1 q_1, \tag{85a}$$

$$\hat{\mathtt{K}}_2 : \quad w = r_2 w_2, \qquad q = r_2. \tag{85b}$$

Chart $\hat{\mathtt{K}}_1$ We insert (85a) in (81) and drop the subscript. We divide the system by the common divisor r to obtain the de-singularized equations:

$$\begin{aligned}
\dot{r} &= r^2 q \left(y + \frac{x+1}{\xi} \right), \\
\dot{x} &= -(x + 1 + \alpha) + xrq \left(y + \frac{x+1}{\xi} \right), \\
\dot{y} &= r + yrq \left(y + \frac{x+1}{\xi} \right), \\
\dot{q} &= q^2(2 - r) \left(y + \frac{x+1}{\xi} \right).
\end{aligned} \tag{86}$$

We have the following:

Lemma 8.3 *In chart* $\hat{\mathtt{K}}_1$ *there exists an attracting 3-dimensional center manifold:*

$$x = -1 - \alpha + \mathrm{O}(r + q), \tag{87}$$

whose intersection with the plane $r = q = 0$ *corresponds to the line* L_0 (54a)*. The trajectory* $\gamma^{1,2}$ *defined in* (56) *connects the point* (83) *to* Q^2 (53a) *along a stable fiber.*

Proof The vector field (86) has a line of fixed points for $r = q = 0, x = -1-\alpha, y \in \mathbb{R}$. This line corresponds to L_0 through the coordinate changes (64b) and (85a). The linearized dynamics around L_0 has only the x-direction that is hyperbolic and that is furthermore stable. Therefore the center manifold (87) appears for r, q sufficiently small. The fixed point (83) in chart $\hat{\mathtt{K}}_1$ becomes:

$$(r, x, y, q) = (0, -1, 0, 0), \tag{88}$$

hence there is a solution backwards asymptotic to (88) and forward asymptotic to the point $Q^2 \in L_0$ through a stable fiber. We denote this connection by $\gamma^{1,2}$. □

By substituting (87) into (86) we obtain the dynamics on the center manifold:

$$\begin{aligned}
\dot{r} &= r^2 q \left(y - \frac{\alpha}{\xi}\right)(1 + \mathrm{O}(r+q)), \\
\dot{y} &= r + yrq \left(y - \frac{\alpha}{\xi}\right)(1 + \mathrm{O}(r+q)), \\
\dot{q} &= q^2(2-r) \left(y - \frac{\alpha}{\xi}\right)(1 + \mathrm{O}(r+q)).
\end{aligned} \tag{89}$$

The line L_0 corresponds to $r = q = 0$. This is a line of non-hyperbolic fixed points, since each point has a triple zero eigenvalue. We gain hyperbolicity of L_0 by introducing the blow-up map :

$$r = \rho\sigma, \quad q = \rho, \tag{90}$$

and divide the resulting vector field by the common divisor ρ to obtain:

$$\begin{aligned}
\dot{\sigma} &= \sigma(-2 + \rho\sigma + \rho^2) \left(y - \frac{\alpha}{\xi}\right)(1 + \mathrm{O}(\rho)), \\
\dot{y} &= \sigma + y\rho\sigma \left(y - \frac{\alpha}{\xi}\right)(1 + \mathrm{O}(\rho)), \\
\dot{\rho} &= \rho(2 - \rho\sigma) \left(y - \frac{\alpha}{\xi}\right)(1 + \mathrm{O}(\rho)).
\end{aligned} \tag{91}$$

Lemma 8.4 *System (91) has two invariant planes for $\rho = 0$ and $\sigma = 0$. On the plane $\sigma = 0$ the solution contracts towards the fixed point at the origin along the trajectory:*

$$\gamma_1^1 := \left\{(\sigma, y, \rho) \in \mathbb{R}^2 \times \mathbb{R}^+ | \quad \sigma = 0, y = 0, \rho \geq 0\right\}. \tag{92}$$

On the plane $\rho = 0$ there is a trajectory that is backwards asymptotic to the origin and forward asymptotic to the point:

$$(\sigma, y, \rho) = (0, 2\alpha/\xi, 0), \tag{93}$$

corresponding to the trajectory $\gamma^{2,4}$ introduced in (56). This trajectory has the explicit solution:

$$\left\{(\sigma, y, \rho) \in \mathbb{R}^2 \times \mathbb{R}^+ | \quad \sigma = 2\frac{\alpha}{\xi} y - y^2, y \in (0, 2\alpha/\xi), \rho = 0\right\}. \tag{94}$$

The invariant trajectory γ_1^2 on the plane $\sigma = 0$:

$$\gamma_1^2 := \left\{(\sigma, y, \rho) \in \mathbb{R}^2 \times \mathbb{R}^+ | \quad \sigma = 0, y = 2\alpha/\xi, \rho \geq 0\right\}, \tag{95}$$

is backwards asymptotic to the point (93) and expands for positive values of ρ.

The results of Lemma 8.4 are summarized in Figure 15.

Remark 8 *The fixed point at the origin of system* (91) *and the point* (93) *correspond to the blow-up of the points* Q^2 *and* Q^4 *respectively while the segment* (94) *corresponds* $\gamma^{2,4}$ *through the blow-up* (90).

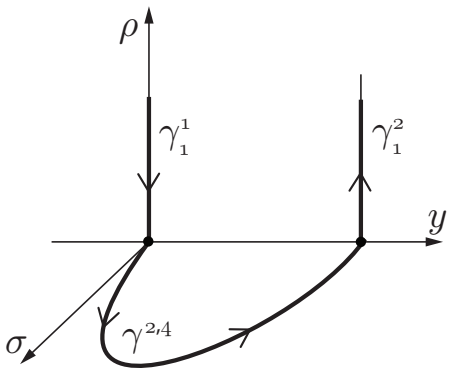

Figure 15: Dynamics in chart $\hat{\mathtt{K}}_1$. The plane $\rho = 0$ corresponds to the blown-up line L_0.

Proof On the plane $\sigma = 0$ we have the following dynamics:

$$\begin{aligned} \dot{y} &= 0, \\ \dot{\rho} &= 2\rho \left(y - \frac{\alpha}{\xi} \right) (1 + \mathrm{O}(\rho)), \end{aligned} \tag{96}$$

therefore the solution contracts towards $\rho = 0$ by following the trajectory γ_1^1 (92). On the plane $\rho = 0$ we obtain:

$$\begin{aligned} \dot{\sigma} &= -2 \left(y - \frac{\alpha}{\xi} \right), \\ \dot{y} &= 1, \end{aligned} \tag{97}$$

where we have divided the right hand side by σ. The solution of (97) with initial condition in the origin is (94). This trajectory is forward asymptotic to (93) along the invariant plane $\sigma = 0$. From this point the variable ρ expands on the invariant line (95) following (96). □

The invariance of the line γ_1^2 in (96) persists in the blown-down chart $\hat{\mathtt{K}}_1$. Therefore we continue the analysis on chart $\hat{\mathtt{K}}_2$ defined in (85b) so that we can describe the

behaviour of the dynamics for large values of q. We de-singularize the vector field by dividing by the common divisor r_2. We find that there are two invariant planes for $r_2 = 0$ and $w_2 = 0$. The trajectory γ_1^2 enters chart $\hat{\mathrm{K}}_2$ on the plane $r_2 = 0$ and contracts towards the origin. We continue this trajectory by following the unstable manifold of the origin on the plane $w_2 = 0$. Here we exit the chart $\hat{\mathrm{K}}_2$ with r_2 large. Consequently we blow-down the orbit to chart $\mathcal{K}_2$ using the map (85b). We enter chart $\mathcal{K}_2$ with $w = 0$ and q large. Therefore the solution of (81) evolves on an invariant line with q increasing. Eventually the chart $\mathcal{K}_2$ is no longer suited to describe the trajectory. Hence we use (68) to move back to chart $\mathcal{K}_1$. We rewrite the dynamics along chart $\mathcal{K}_1$ in the old coordinate x (see (65)) and obtain:

$$\begin{aligned}
\dot{w} &= w^2 \left(y + \frac{x+1}{\xi} \right), \\
\dot{x} &= -\epsilon w(x + 1 + \alpha) + xw \left(y + \frac{x+1}{\xi} \right), \\
\dot{y} &= \epsilon w^2 + yw \left(y + \frac{x+1}{\xi} \right), \\
\dot{\epsilon} &= -2\epsilon \left(y + \frac{x+1}{\xi} \right).
\end{aligned} \tag{98}$$

The trajectory γ_1^2 becomes in chart $\mathcal{K}_1$:

$$\mathcal{K}_{21}(\gamma_1^2) := \left\{ (w, x, y, \epsilon) \in \mathbb{R}^+ \times \mathbb{R}^2 \times \mathbb{R}^+ | \quad w = 0, x = -1 - \alpha, y = \frac{2\alpha}{\xi}, \epsilon \geq 0 \right\}. \tag{99}$$

We notice that the variable ϵ decreases exponentially. We therefore consider $\epsilon = w = 0$ in (98) and divide the right hand side by w to obtain the de-singularized layer problem:

$$\begin{aligned}
\dot{x} &= x \left(y + \frac{x+1}{\xi} \right), \\
\dot{y} &= y \left(y + \frac{x+1}{\xi} \right),
\end{aligned} \tag{100}$$

within $w = 0$. Therefore from Q^4 we follow the fast fiber $\gamma^{4,5}$ introduced in (57). This fiber is a solution of the layer problem (100) and contracts to the point Q^5 on C_0. Since Q^5 may not be visible in chart K_3, we compute its coordinates in chart K_1.

8.2. Chart K_1

We insert (51b) into the fast problem (49) and divide by e^{z_1/w_1} to obtain the desingularized vector field in chart K_1. We drop the subscript henceforth for the sake of readability:

$$\begin{aligned} \dot{w} &= -\varepsilon w^2(1-\mathrm{e}^{-z/w}), \\ \dot{x} &= -\varepsilon\left(x+(1+\alpha)z\right) - \varepsilon x w(1-\mathrm{e}^{-z/w}), \\ \dot{z} &= -\mathrm{e}^{-2z/w}\left(1+\frac{x+z}{\xi}\right) - \varepsilon z w(1-\mathrm{e}^{-z/w}). \end{aligned} \tag{101}$$

In chart K_1 the layer problem is:

$$\begin{aligned} \dot{w} &= 0, \\ \dot{x} &= 0, \\ \dot{z} &= -\mathrm{e}^{-2z/w}\left(1+\frac{x+z}{\xi}\right), \end{aligned} \tag{102}$$

therefore the fibers are all vertical and in particular the fiber $\gamma^{4,5}$ is written as in (57) since it departs from $K_{31}(Q^4)$. Hence $\gamma^{4,5}$ is forward asymptotic to the point:

$$Q^5 = \quad (w,x,z) = \left(0, -\frac{\xi}{2\alpha}(1+\alpha), \frac{\xi}{2\alpha}(1-\alpha)\right). \tag{103}$$

Figure 10(c) illustrates the dynamics in chart K_1. We remark that the change of coordinates from chart K_3 to chart K_1 is defined for $z_1 > 0$ and therefore for $\alpha > 1$ the point Q^5 is not visible in chart K_3. The point Q^5 is connected to Q^6 through the segment $\gamma^{5,6}$ that follows directly from the analysis of the reduced problem of section 5. From the point Q^6 the solution is connected to the point Q^1 through the manifold $W^{c,u}$.

8.3. Collecting the results

To prove the Conjecture 7.1 we would have to consider a section $\Lambda_1 := \{w_1 = \delta\}$ transverse to $W^{c,u}$ where $\delta > 0$ is small but fixed. Using the blow-up in chart K_3 we can track a full neighbourhood of $\Lambda_1 \cap W^{c,u}$ using Proposition 5.2, $\gamma^{1,2}, \gamma^{2,4}, \gamma^{4,5}, \gamma^{5,6}$ and $W^{c,u}$ respectively, to obtain a return map $P_1 : \Lambda_1 \to \Lambda_1$. For $\varepsilon = 0$ the forward flow of a neighborhood of $\Lambda_1 \cap W^{c,u}$ contracts to the point Q^1. This would provide the desired contraction of P_1 and establish, by the contraction mapping theorem, the existence of the limit cycle Γ_ε satisfying $\Gamma_\varepsilon \to \Gamma_0$ for $\varepsilon \to 0$.

9. Conclusions

In this paper we have considered the one dimensional spring-block model that describes the earthquake faulting phenomenon. We have used geometric singular perturbation theory and the blow-up method to provide a detailed description of the periodicity of the earthquake episodes. In particular we have shown that the limit cycles arise from a degenerate Hopf bifurcation. The degeneracy is due to an underlying Hamiltonian structure that leads to large amplitude oscillations. Using the Poincaré compactification together with the blow-up method, we have described how these limit cycles behave near infinity in the limit of $\varepsilon \to 0$. A full detailed proof of Conjecture 7.1, including the required careful estimation of the contraction, will be the subject of a separate manuscript.

We are optimistic that we can extend the machinery used in this paper to the two degrees of freedom model presented by Erickson et al. (2011), in particular to study the Heaton pulses (Heaton 1990). Moreover we expect that our method can be extended to study the one dimensional spring-block model when the Dieterich state law is considered instead of the Ruina one. Our analysis suggests suitable coordinate sets and time rescales to deal with the stiffness of the problem during numerical simulations. We hope that a deeper understanding of the structure of the earthquake cycles may be of help for the temporal predictability of the earthquake episodes.

Acknowledgments

The first author thanks Thibault Putelat and Björn Birnir for the useful discussions. We acknowledge the Idella Foundation and the Centre de Recerca Matematica (CRM) in Barcelona for supporting the research.

References

Belardinelli M E & Belardinelli E 1996 *Nonlinear Processes in Geophysics* **3**(3), 143–149.
Ben-Zion Y 2008 *Reviews of Geophysics* **46**(4). RG4006.
Bizzarri A 2010 *Geophysical Research Letters* **37**(20). L20315.
Burridge R & Knopoff L 1967 *Bulletin of the Seismological Society of America* **57**(3), 341–371.
Carlson J M & Langer J S 1989 *Physical Review A* **40**(11), 6470–6484.
Carlson J M, Langer J S, Shaw B E & Tang C 1991 *Physical Review A* **44**(2), 884–897.
Chow S N, Li C & Wang D 1994 *Normal Forms and Bifurcation of Planar Vector Fields* Cambridge University Press.

Corless R M, Gonnet G H, Hare D E G, Jeffrey D J & Knuth D E 1996 *Advances in Computational Mathematics* **5**(1), 329–359.
Dieterich J H 1972 *Journal of Geophysical Research* **77**(20), 3690–3697.
Dieterich J H 1978 *Pure and Applied Geophysics* **116**(4-5), 790–806.
Dieterich J H 1979 *Journal of Geophysical Research* **84**(B5), 2161–2168.
Dumortier F & Roussarie R 1996 *Memoirs of the American Mathematical Society* **121**(577).
Eckhaus W 1973 *Matched asymptotic expansions and singular perturbations* North-Holland Publ.
Erickson B, Birnir B & Lavallée D 2008 *Nonlinear Processes in Geophysics* **15**(1), 1–12.
Erickson B, Birnir B & Lavallée D 2011 *Geophysical Journal International* **187**(1), 178–198.
Fan Q, Xu C, Niu J, Jiang G & Liu Y 2014 *Journal of Seismology* **18**(3), 637–649.
Fenichel N 1974 *Indiana University Mathematics Journal* **23**(12), 1109–1137.
Fenichel N 1979 *Journal of Differential Equations* **31**(1), 53–98.
Gu J C, Rice J R, Ruina A L & Tse S T 1984 *Journal of the Mechanics and Physics of Solids* **32**(3), 167–196.
Gucwa I & Szmolyan P 2009 *Discrete and Continuous Dynamical Systems - Series S* **2**(4), 783–806.
Heaton T H 1990 *Physics of the Earth and Planetary Interiors* **64**(1), 1–20.
Jones C K R T 1995 *in* R Johnson, ed., 'Dynamical Systems' Vol. 1609 of *Lecture Notes in Mathematics* Springer Berlin Heidelberg pp. 44–118.
Kaper T J 1999 *in* 'Proceedings of Symposia in Applied Mathematics' Vol. 56 American Mathematical Society pp. 85–132.
Kristiansen K U 2016 *ArXiv e-prints arXiv:1603.01821 [math.DS]* .
Krupa M & Szmolyan P 2001 *SIAM Journal on Mathematical Analysis* **33**(2), 286–314.
Kuehn C 2014 *Nonlinearity* **27**(6), 1351–1366.
Kuehn C 2015 *Multiple Time Scale Dynamics* Vol. 191 of *Applied Mathematical Sciences* Springer International Publishing.
Lapusta N, Rice J R, Ben-Zion Y & Zheng G T 2000 *Journal of Geophysical Research* **105**(B10), 23765–23789.
Madariaga R 1998 Complex Heterogeneous Faulting Models. Unpublished notes (Preprint).
Madariaga R & Cochard A 1996 *Proceedings of the National Academy of Sciences of the United States of America* **93**(9), 3819–3824.
Marone C 1998*a* *Nature* **391**(6662), 69–72.
Marone C 1998*b* *Annual Review of Earth and Planetary Sciences* **26**, 643–696.
Marone C, Vidale J E & Ellsworth W L 1995 *Geophysical Research Letters* **22**(22), 3095–3098.
Meiss J D 2007 *Differential dynamical systems* SIAM.
Nadeau R M & McEvilly T V 1999 *Science* **285**(5428), 718–721.
Nakatani M 2001 *Journal of Geophysical Research: Solid Earth* **106**(B7), 13347–13380.
Pomeau Y & Berre M L 2011 *ArXiv e-prints arXiv:1107.3331 [physics.geo-ph]* .
Putelat T, Willis J R & Dawes J H P 2008 *Philosophical Magazine* **88**(28–29), 3219–3243.
Ranjith K & Rice J R 1999 *Journal of the Mechanics and Physics of Solids* **47**(6), 1207–1218.
Rankin J, Desroches M, Krauskopf B & Lowenberg M 2011 *Nonlinear Dynamics* **66**(4), 681–688.
Rice J R & Ruina A L 1983 *Journal of Applied Mechanics* **50**(2), 343–349.
Rice J R & Tse S T 1986 *Journal of Geophysical Research* **91**(B1), 521–530.

Ruina A 1983 *Journal of Geophysical Research: Solid Earth* **88**(B12), 10359–10370.
Vidale J E, Ellsworth W L, Cole A & Marone C 1994 *Nature* **368**(6472), 624–626.
Zechar J D & Nadeau R M 2012 *Geophysical Journal International* **190**(1), 457–462.